BLOWING RATIO EFFECTS ON FILM COOLING EFFECTIVENESS

A Thesis

by

KUO-CHUN LIU

Submitted to the Office of Graduate Studies of
Texas A&M University
in partial fulfillment of the requirements for the degree of

MASTER OF SCIENCE

August 2009

Major Subject: Mechanical Engineering

BLOWING RATIO EFFECTS ON FILM COOLING EFFECTIVENESS

A Thesis

by

KUO-CHUN LIU

Submitted to the Office of Graduate Studies of
Texas A&M University
in partial fulfillment of the requirements for the degree of

MASTER OF SCIENCE

Approved by:

Chair of Committee,	J.C. Han
Committee Members,	S.B. Wen
	H.C. Chen
Head of Department,	Dennis O'Neal

August 2009

Major Subject: Mechanical Engineering

ABSTRACT

Blowing Ratio Effects on Film Cooling Effectiveness. (August 2009)

Kuo-Chun Liu, B.S., Kansas State University

Chair of Advisory Committee: Dr. Je-Chin Han

The research focuses on testing the film cooling effectiveness on a gas turbine blade suction side surface. The test is performed on a five bladed cascade with a blow down facility. Four different blowing ratios are used in this study, which are 0.5, 1.0, 1.6, and 2.0; mainstream flow conditions are maintained at exit Mach number of 0.7, 1.1 and 1.3. Nitrogen is injected as the coolant so that the oxygen concentration levels can be obtained for the test surface. Based on mass transfer analogy, film cooling effectiveness can be computed with pressure sensitive paint (PSP) technique. The effect of blowing ratio on film cooling effectiveness is presented for each testing condition. The spanwise averaged effectiveness for each case is also presented to compare the blowing ratio and mainstream effect on film cooling effectiveness. Results show that due to effects of shock, the optimum blowing ratio is 1.6 for exit Mach number of 1.1 and 1.3; however; without the effects of shock, the optimum blowing ratio is 1.0 for exit Mach number of 0.7.

DEDICATION

To my parents and sister for their endless love, support and encouragement

ACKNOWLEDGEMENTS

I am very grateful to Dr. Je-Chin Han for mentoring me throughout my academic work here at Texas A&M University. He has provided me with invaluable experience as a research assistant in gas turbine studies. I am appreciative of Dr. Sy-Bor Wen and Dr. Hamn-Ching Chen for serving on my committee and offering valuable suggestions to improve my research and reports. I also thank my partners, Michael Hue and Diganta Narzary, who spent lots of time and effort on test section design, assembly and conducting the experiment.

TABLE OF CONTENTS

Page

Page

LIST OF FIGURES

Page

Page

Page

Page

Page

LIST OF TABLES

Page

NOMENCLATURE

A	total film cooling hole area, (m^2)
A_h	single film cooling hole area, (m^2)
C_∞	oxygen concentration of mainstream
C_{mix}	oxygen concentration of mainstream-coolant mixture
C_{N_2}	oxygen concentration of nitrogen
DR	density ratio
I	momentum ratio
$I(P)$	emission intensity of PSP
$I(P)_{ref}$	emission intensity of PSP at reference (atmospheric) pressure
$I(P)_{black}$	emission intensity of PSP at no-flow and without light excitation
M	blowing ratio
$\dot{m}$	mass flow rate, (kg/s)
n	number of film cooling holes
$(P_{O_2})_{air}$	partial oxygen pressure in air, (Pa)
$(P_{O_2})_{mix}$	partial oxygen pressure in coolant-air mixture, (Pa)
T	temperature, (K)
T_c	coolant temperature, (K)
T_∞	mainstream temperature, (K)
V_c	average coolant velocity, (m/s)

V_m	mainstream velocity, (m/s)
Q_c	volumetric flow rate of coolant, (m^3/s)
γ	specific heat ratio
η	film cooling effectiveness
ρ_c	coolant density, (kg/m^3)
ρ_m	mainstream density, (kg/m^3)

INTRODUCTION AND LITERATURE REVIEW

The gas turbine industry engineers are always trying to increase the turbine inlet temperature due to its significant promotion to thrust and thermal efficiency. However, a high inlet temperature will induce some major problems to the turbine blade. For example, the design operating temperature of turbine is above melting temperature of the material; therefore, the blade is not able to withstand such high temperatures and thermal stresses. In modern gas turbine technology, numerous cooling techniques have been developed to prevent the blade and vane from damage. Han et al. [1] describes many cooling techniques that are commonly used in various combinations to increase the lifetime of the turbine blade. Internal cooling method, including impingement cooling, rib-turbulated cooling, and pin-fin cooling, is used to remove heat from the inside of the blade. Figure 1 shows the typical cooling methods of modern gas turbine blades. External cooling method is mostly focused on film cooling technique, in which cool air is bled from the compressor stage, ducted to the internal chambers of the turbine blades, and discharged through small holes in the blade walls into the hot mainstream. The discharged coolant air provides a thin, relatively cool layer on the outer surface of the blade and functions as an insulator. After all, the blade is able to withstand the extremely hot mainstream gases and has a longer lifetime cycle.

This thesis follows the style of ASME Journal of TurboMachinery.

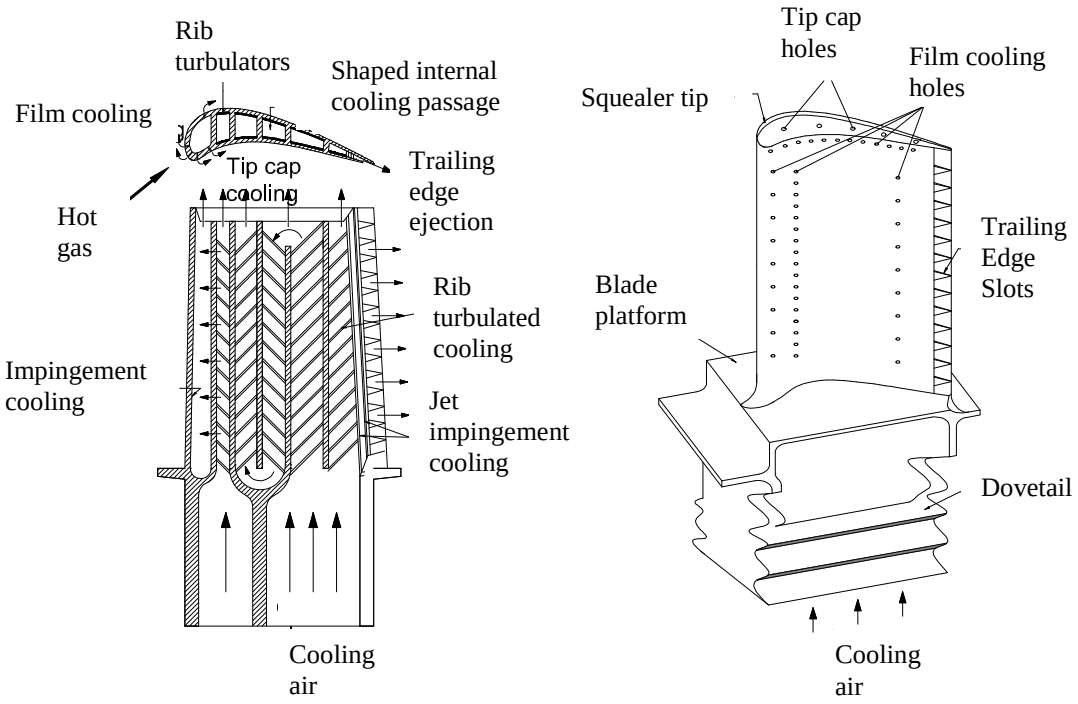

Fig. 1 Blade cooling techniques

Film cooling technique is facing two major issues: (1) when we supply too much coolant into the film cooling chamber, instead of forming a thin layer and attaching on the blade surface, it will penetrate into the mainstream. Thus, the blade losses the protection and has no cooling effectiveness, and (2) the space between two discrete cooling holes is not covered well by the coolant layer. Above situations causes hot spots on the blade surface and results a non-uniform cooling distribution.

Engineers are always trying to maximize the cooling efficiency by using less coolant and have optimum cooling results. Designers and researchers discovered that injection hole geometry has a significant effect on cooling efficiency.

Among the variety of film cooling hole designs, compound angle and shaped holes are generally considered in modern high pressure and high temperature gas turbine engines. Figure 2 shows the schematic hole geometries and the cross section view cutting along the hole centerline. The compound angle hole provides better effectiveness as the coolant is deflected by the mainstream and covers a wider area. The shaped hole performs better because the expanded diffused area reduces the jet momentum and prevents the coolant separate from the blade surface.

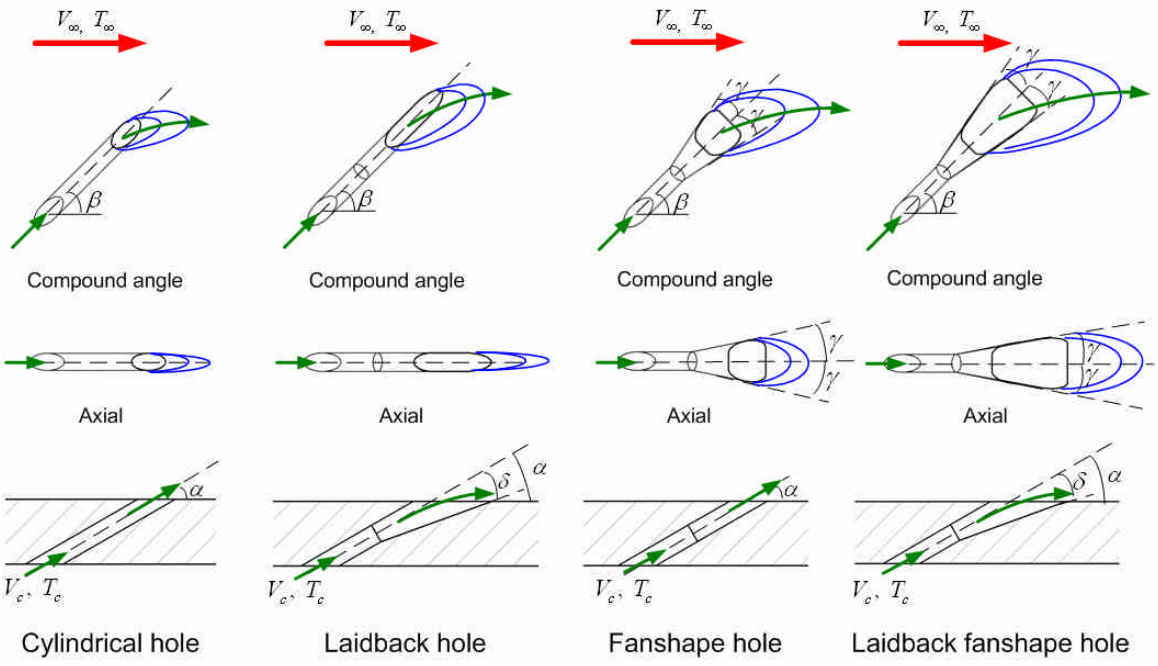

Fig. 2 Compound angle and different shaped hole

Injection Hole Shape

There are many experimental studies focusing on different hole configurations and geometries. Goldstein et al. [2] were the first to investigate the shaped injection holes to improve film cooling performance. They compared the film cooling effectiveness for cylindrical holes and axial fanshaped hole with lateral diffusion of 10 º. They determined a significant improvement of film cooling effectiveness and coolant coverage of the shaped hole.

Sen et al. [3] and Schmidt et al. [4] studied forward diffused holes. They discovered that the 15º forward diffused holes also provide better effectiveness than cylindrical holes. Thole et al. [5] measured the flow fields for three types of injection holes: a cylindrical hole, a laterally diffused hole, and a forward-laterally diffused hole. Their results showed that diffusing the injection hole reduces the coolant penetration into the mainstream and reduces the intense shear regions when compared to cylindrical holes. Gritsch et al. [6] studied the same cooling hole configuration and orientation as [5] with a density ratio of 1.85. As compared to cylindrical hole, both shaped holes showed significant improved thermal protection of the surface downstream of the ejection location.

Yu et al. [7] studied film cooling effectiveness and heat transfer distributions on a flat plate with cylindrical hole, laidback hole, and laidback shaped hole. The laidback

shaped hole provided the highest film cooling effectiveness and overall heat transfer reduction.

In 2007, Gao et al. [8] studied the film effectiveness laidback fanshape hole geometries with compound angles using the PSP technique. The coolant is only injected to either pressure side or suction side of the blade. Upstream wake simulation is done by placing a periodic set of rod upstream of the test blade. The free stream Reynolds number, based on the axial chord length and the exit velocity, is 750,000 and the inlet and exit Mach numbers are 0.27 and 0.44. They investigated that laidback fanshape holes with compound angle provide very good coolant t film coverage on the suction side. Overall, the compound angle shaped holes perform the much better than compound angle cylindrical holes by expanding diffused area.

Effects of Blowing Ratios

Blowing ratio is defined as mass flux ratio between coolant and mainstream. This has been extensively studied to maximize the film cooling effectiveness. Optimizing the blowing ratio is important, because low blowing ratio would not provide enough coolant to cover the blade surface effectively; however, blowing ratio is too high causes the coolant shoot into the mainstream. Studies have also shown the optimum blowing ratios are not the same for every hole shape.

Goldstein et al. [2, 9] showed cylindrical holes have the optimum blowing ratio abound M = 0.5. The higher blowing ratios cause coolant jets penetrated into the mainstream and reduce the cooling effectiveness. Further downstream the effectiveness tended to increase with the blowing rate where the coolant jets reattached to the surface.

Cho et al. [10] compared the blowing ratio effects for two different types of hole shapes. (1) diffused 4 º in all direction, (2) forward diffusion of 8 º. As blowing ration increases, the coolant becomes more separate from the surface and reduces the cooling effectiveness. The optimum blowing ratio for cylindrical hole in this study is closed to M = 0.5. Shaped hole #1 also showed decreasing effectiveness for increasing blowing ratios. However, film cooling effectiveness values did not drop till M = 1.0. Shaped hole #2 performed similarly when compared to the other holes. At the highest blowing ratio of M = 2.0, the effectiveness distribution was more similar to the cylindrical hole rather than the shaped hole #1. Because this hole has an expansion in the forward direction only, the diffusion of coolant in the hole is not uniform. Therefore the interaction between the mainstream and the coolant is stronger.

Gao et al. [8] studied film cooling effectiveness distribution on the blade pressure side or suction side with axial hole without showerhead film cooling. Their results showed the moderate blowing ratios M = 0.6 to 1.2 gave better film cooling effectiveness. Further increasing blowing ratio to M = 1.5, the effectiveness decreases because coolant jet liftoff.

Free-Stream Turbulence Effects

Turbulence is generated by using grids upstream of the test section, the grid functions as a blockage to the flow. Jet grids are also used to generate free stream turbulence. Air is forced through an array of pipes into mainstream. At the exit of combustor, the turbulence intensity is about 7 to 20%; thus, the first stage vane can have the turbulent inlet boundary condition as high as 20%.

Saumweber et al. [11] found that the free stream turbulence in tensity is reduced because of air accelerates through the vane. Free-stream turbulence levels at engine conditions can therefore be in the range of 8 to 12%.

Kadotani and Goldstein [12, 13] tested turbulent intensities ranging form 0.3 to 20.6% with length scales between 0.06 and 0.33 cylindrical holes inclined 33º to the mainstream. At low blowing ratio, high turbulent intensities produced a decrease in centerline effectiveness. At high blowing ratio, however, high turbulence increased the centerline effectiveness. This was because the turbulent mixing reduced the penetration of the coolant into the mainstream. Additionally, the high turbulence improved the lateral distribution of the coolant for the cylindrical holes. Low turbulence, however, creates a more uniform lateral distribution of effectiveness.

Mehendal and Han [14] studied the high turbulence intensity effect on the turbine blade leading edge. They measured the cooling effectiveness on the semicircular leading edge

with flat downstream body by using thermal couples. The blowing ratio was varied from 0.4 to 1.2 for different free stream turbulence levels. High turbulence intensity was generated by passive grid (9.67%) and jet grid (12.9%). They found that the free stream turbulence reduces the film cooling effectiveness at blowing ratio of 0.4. Higher free stream turbulence intensity causes coolant jet to dissipate into the mainstream faster. Beside, the unsteady mainstream penetrates and mixes with film cooling layer and reduces the effectiveness. The coolant jet attaches on the blade surface and maintained over a long distance when turbulence intensity is low, and provides higher effectiveness. By increasing the coolant ratio, the coolant jet momentum is stronger and unsteady mainstream causes fewer disturbances. Therefore it has less turbulence effect on high blowing ratio film cooling effectiveness.

Burd et al. [15] had an important founding that the L/D ratio of the film cooling hole has to be taken into account when comparing turbulent intensity effects on film cooling. They measured mainstream turbulence intensity by using hot wire anemometer on cylindrical holes angled 35º to the mainstream. Two turbulent intensities (0.5 and 12%) while varying the L/D ratio from 2.3 to 7 had been tested. With low free-stream turbulence and short holes, the coolant is ejected farther from the wall and spreads more in the spanwise direction when compared to a long hole. At high free-stream turbulence, though, the flow differences between a long and short hole greatly decrease

Gao et al. [16] took the measurement in a five-bladed linear cascade facility. They used metal rods placed periodically upstream of the test blade to simulate the stationary, upstream wake. The rods were placed upstream of the blades at the 50% axial chord length. Rods locations for 0%, 25%, 50% and 75% were progressively located along the blade pitch-wise direction. They concluded that the wake rod locations of 0% and 25% significantly decrease the film cooling effectiveness; however, wakes from 50% and 75% locations may not attach to the blade surfaces and hence do not impact the film cooling effectiveness as much.

Effects of Density Ratios

In real engines, the coolant to mainstream density ratio is close to 2. Because the coolant is at lower temperature and higher pressure than the mainstream, which causes the density difference. Rather than using nitrogen to be the coolant, which has similar molecular weight as air, other gases have greater molecular weight are considered to be used.

Pedersen et al. [17] investigated the effect of blowing ratio of film cooling effectiveness. They tested various density ratios from 0.75 to 4.17. They found out as density ratio increases, the peak on cooling effectiveness moves toward to higher blowing ratio. Thus, they concluded that greater density ratio coolant tends to attach closer to the blade surface compared to the light density ratio coolant at the same blowing ratio.

Sinha et al. [18] studied similarly on various density ratio coolants under different blowing ratio. For a constant density ratio, the film cooling effectiveness reaches a peak as blowing ratio increases and starts to drop off at very high blowing ratio. This is because the coolant ejection penetrates through the mainstream and losses the protection of the blade surface. Peaks move toward higher blowing ratio by increasing density ratio and provide higher effectiveness. Because of less mixing and lower momentum, the higher density coolants stay closer to the surface. They also shows the film effectiveness with momentum flux ratio, since momentum flux ratio is the combination of blowing ratio and density ratio, it scales the better effects on film effectiveness.

Effects of Tip Leakage

In most experimental studies, blade film cooling is focused on the mid-span region only; the effects of endwall and tip leakage were not captured. Mhetras and Han [19] obtained detailed film cooling effectiveness distribution on a fully film cooled blade surface by using PSP technique. There are three showerhead rows of cylindrical holes with an angle of 30 in radial direction in the leading region. There were compound angle holes on the blade surface, four rows on the pressure side and two rows on the suction sides. During the test, all holes are opened. They showed that the coolant on the suction side was swept toward the mid-span region due to tip leakage vortices and endwall vortices. Blowing ratios are varied from M = 0.3 to M = 1.2, results showed the compound angle cylindrical hole obtained highest cooling effectiveness at M = 0.9. In another paper, Mhetras and Han [20], they studied the upstream film cooling accumulation effect on the

downstream film cooling using superposition method. Four rows and two rows of compound angle cylindrical holes were arranged on the pressure and suction sides. Results showed the film cooling effectiveness on the suction side is much higher than the pressure side. Superposition from individual cooling rows shows good agreement with experimental data.

OBJECTIVES

The research focuses on testing the film cooling effectiveness on a gas turbine blade suction side surface for different blowing ratios and mainstream velocities. Test is performed on a five bladed cascade with a blow down facility. Based on mass transfer analogy, film cooling effectiveness is measured with pressure sensitive paint (PSP) technique. Test vane has three rows of cylindrical holes on the leading edge, and two rows of compound angle shaped holes on the suction side. Each row has total 7 film cooing holes. Four different blowing ratios are used in this study, which are 0.5, 1.6, 2.0 and 3.0. Experiment is operated under three mainstream flow conditions, one is with subsonic exit velocity as Mach number = 0.7 and the others are with supersonic exit velocities as Mach number = 1.1 and 1.3.

INSTRUMENTATION

The experiment is tested in the test section consisted of a stationary blow-down facility with a five-bladed annular cascade. Figure 3 shows the schematic setup of blow down facility and digital controllers. Compressed air store in the tanks entered a high flow pneumatic control valve that was designed to receive feedback from the downstream pressure to mainstream a velocity within ±3% of the desired value. The inlet and exit transition dusts of the test section had inner diameter of 4 inch and were made of 0.125 inch thick aluminum.

As shown in Figure 4, the cascade was made of Selective Laser Sintering (SLS). A viewing window was made of transparent Stereolithograpgy (SLA) and was installed above the test vane, a SLS strip was attached with the window in order to provide additional reinforcement. In the cooling effectiveness test, a 12-bit, scientific grade CCD camera (Cooke Sensicam QE with CCD temperature maintained at -15°C using 2-stage peltier cooler) and a strobe light (PerkinElmer MVS-7000 Series) fitted with a narrow band-pass filter (optical wavelength = 520 nm) were placed above the viewing window. A turbulence grid was installed upstream of the test section.

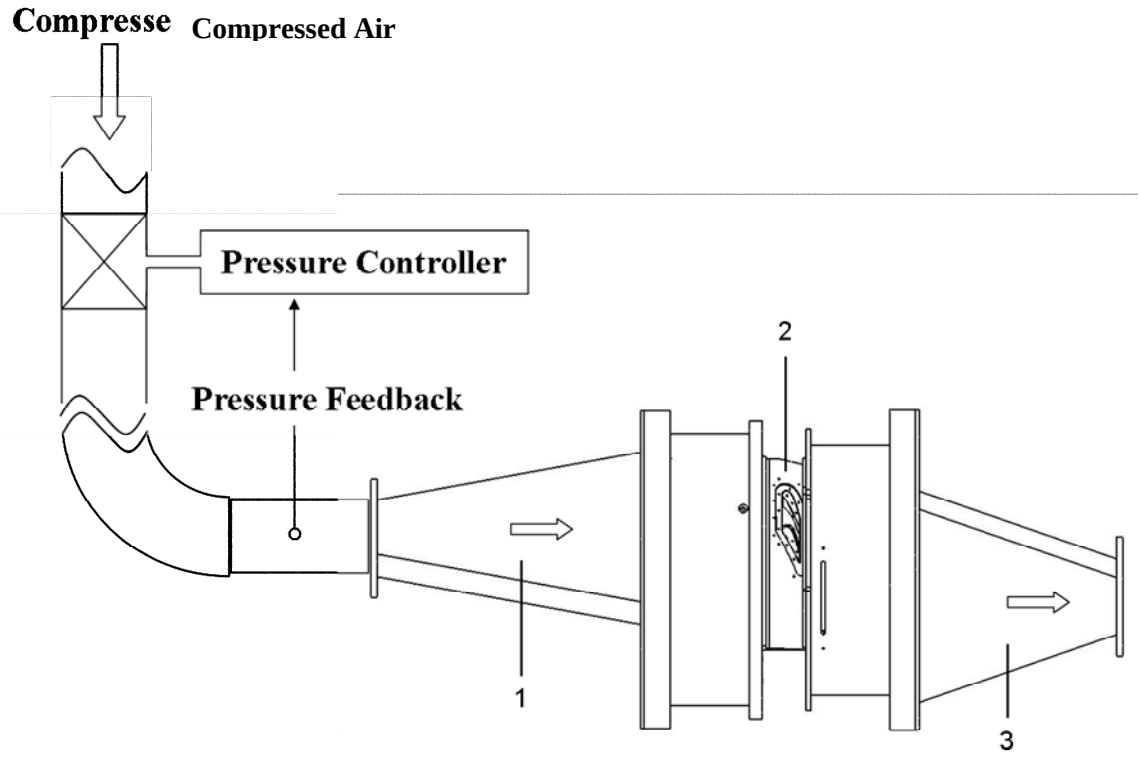

1. **Inlet Transition Duct**
2. **Cascade**
3. **Exit Transition Duct**

Fig. 3 Schematic of blow down facility and digital controller setup

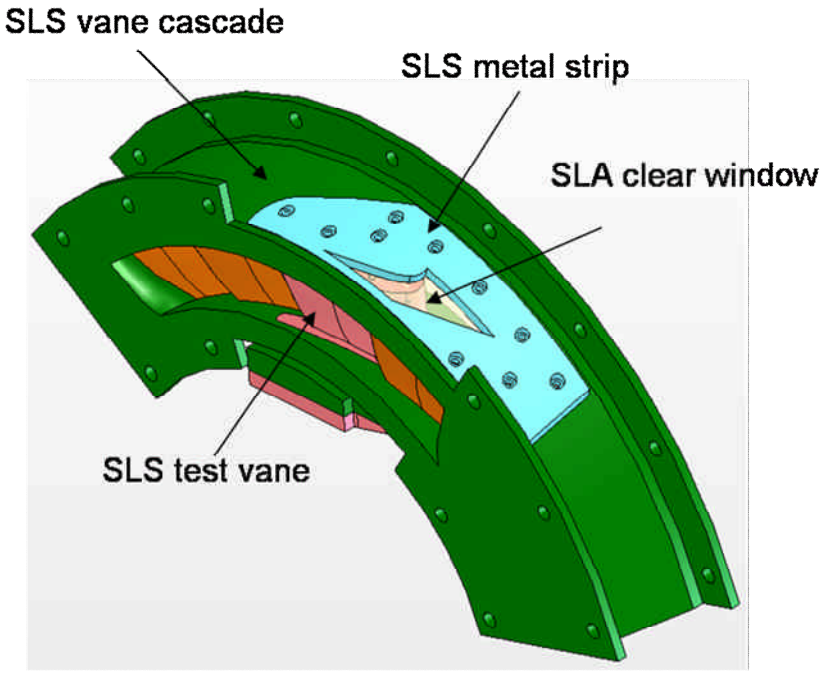

Fig. 4 Test section cascade assembly

Pitot tubes are placed at the inlet and the exit of the test section to measure the total and static pressures. Coolant is ejected to leading edge (3 rows of cylindrical holes) and suction side (2 rows of compound angle shaped holes); three ASME Orifice flow meters are used to control the coolant volumetric flow rate and adjust the blowing ratios. Static pressure taps are attached at the flow meter exit to measure the coolant pressure. The entire experimental setup, including cascade, coolant supply and camera position are shown is Figure 5.

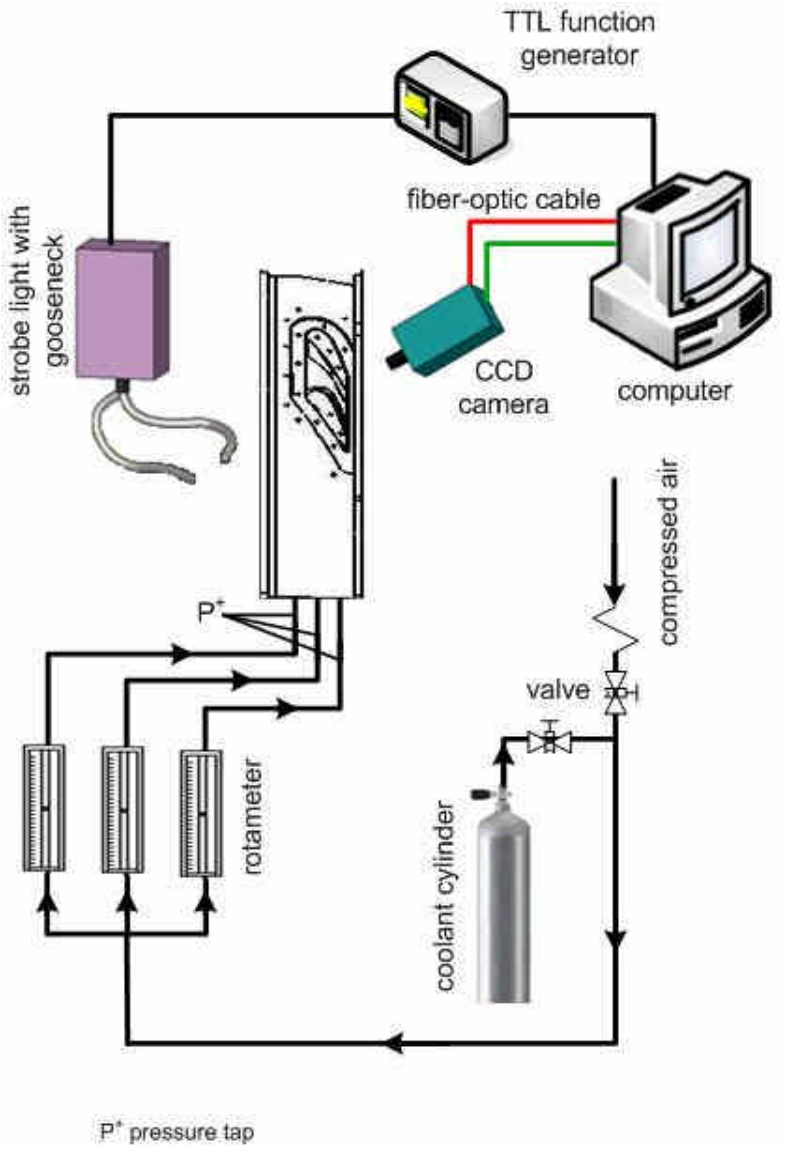

Fig. 5 Schematic of experimental facility

During the blow down test, the cascade exit air velocities are maintained at Mach number 0.7, 1.1 and 1.3, respectively. The corresponding Reynolds numbers based on axial chord length and exit mainstream velocity are 6.33×10^5, 9.98×10^5 and 1.18×10^6.

Test vane was made of SLS and its height decreases from the leading edge to trailing edge as of 5.85 cm to 4.63 cm. The axial chord length of the blade is 3.96 cm. The blade has 3 rows of cylindrical film cooling holes on leading edge, and 2 rows of compound angle shaped holes on suction side surface. Each row has total 7 film cooling holes as shown in Figure 6. Cylindrical holes have a 15.8° incline angle with respect to vertical direction, and the compound angle shaped holes held an angle of 15.8° to the axial direction. As shown in Table 1, the experiments are tested under blowing ratio of 0.5, 1.0, 1.6 and 2.0 with exit Mach number of 0.7, 1.1 and 1.3.

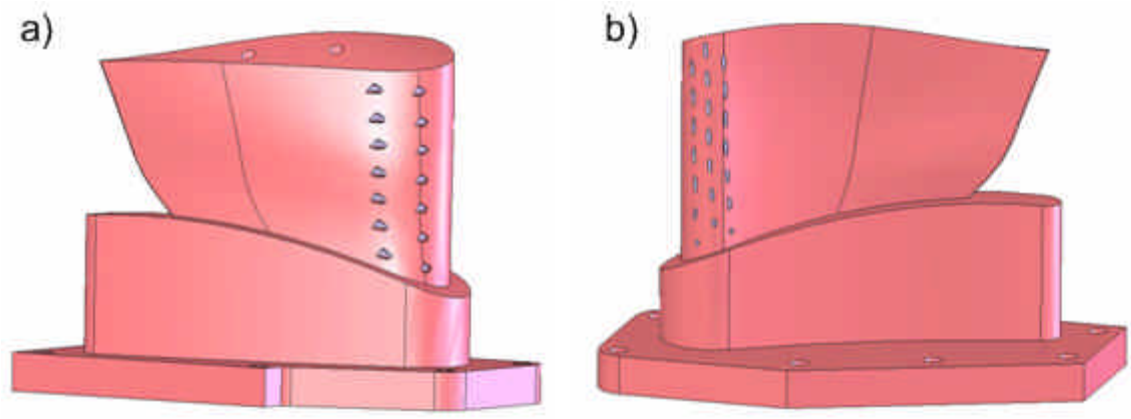

Fig. 6 Drawing of test vane (a) suction side, (b) pressure side

Table 1. Summary of experimental conditions

Expt.	Exit Mach Number	Blowing Ratio	Coolant
1	0.7	0.5	N_2
2	0.7	1.0	N_2
3	0.7	1.6	N_2
4	0.7	2.0	N_2
5	1.1	0.5	N_2
6	1.1	1.0	N_2
7	1.1	1.6	N_2
8	1.1	2.0	N_2
9	1.3	0.5	N_2
10	1.3	1.0	N_2
11	1.3	1.6	N_2
12	1.3	2.0	N_2

DATA REDUCTION

The method used to calculate the film cooling effectiveness is called pressure sensitive paint (PSP). An overview of the effectiveness measuring techniques is found in Han et al. [1]. Film cooling involves the mainstream temperature (T_m), the coolant temperature (T_c), and the film temperature (T_f). Figure 7 shows a diagram for the three temperatures involved in film cooling. The efficiency of film cooling is quantified by a parameter known as film cooling effectiveness, η. It is defined in Equation 1.

$$\eta = \frac{T_f - T_m}{T_c - T_m} \tag{1}$$

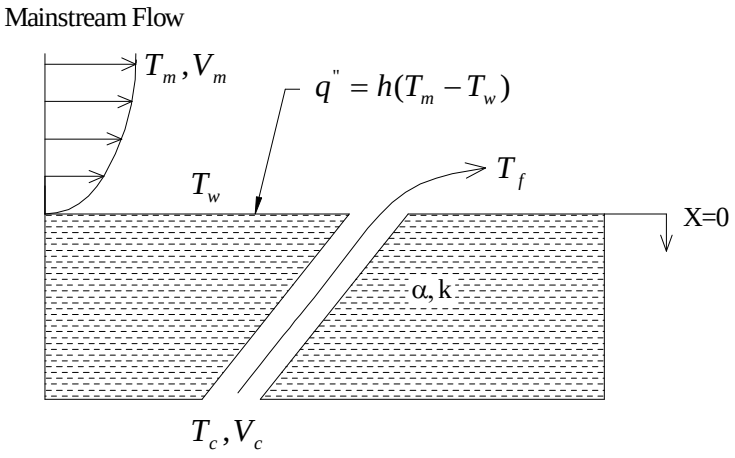

Fig. 7 Three temperature model for film cooling effectiveness

Pressure Sensitive Paint Technique

Data for film cooling effectiveness were measured using the PSP technique. Several authors such as Han et al. [1], Zhang and Jaiswal [35], and Zhang and Fox [36] have discussed this type of technology. A basic PSP setup is shown in Figure 8. PSP is formed from a polymer binder with luminescent molecules suspended in the binder. This binder is permeable, allowing oxygen molecules to penetrate into the paint, and interact with the luminescent molecules. A light source excites the molecules, and when the molecules return to their ground state, a longer wavelength luminescent light is emitted through a process called fluorescence. The premise behind PSP is an oxygen quenching effect. As the oxygen partial pressure of the gas in direct contact with the surface increases, the intensity of the light emitted by the PSP decreases (hence, oxygen quenched).

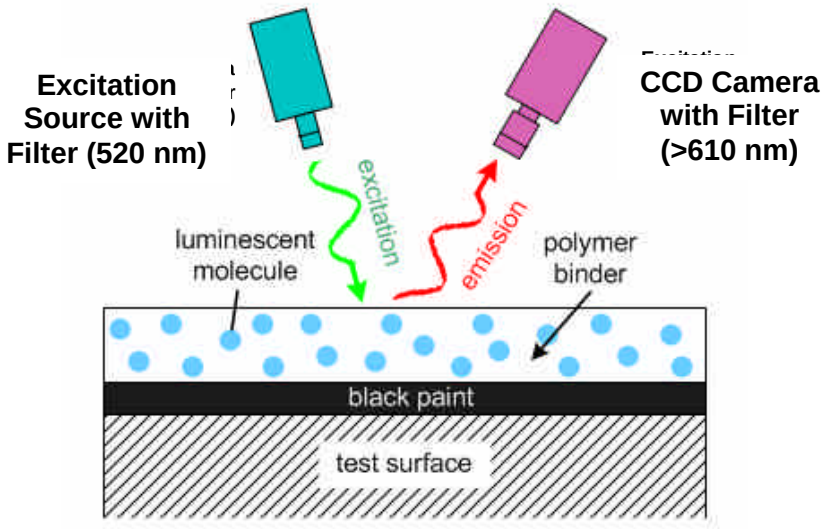

Fig. 8 A basic PSP setup

Calibration of PSP system was performed using a vacuum chamber at several known pressure varying form 0 to 1 atm. A test plate is sprayed with the Uni-FIB PSP (UF470-750) supplied by Innovative Scientific Solutions, Inc. (ISSI) and placed inside the chamber as shown in Figure 9. At each measurement point, the PSP sample is excited using a strobe light equipped with a 500 nm broadband pass filter. A 12-bit, scientific grade CCD camera with a 630 nm filter records the intensity emitted by the PSP.

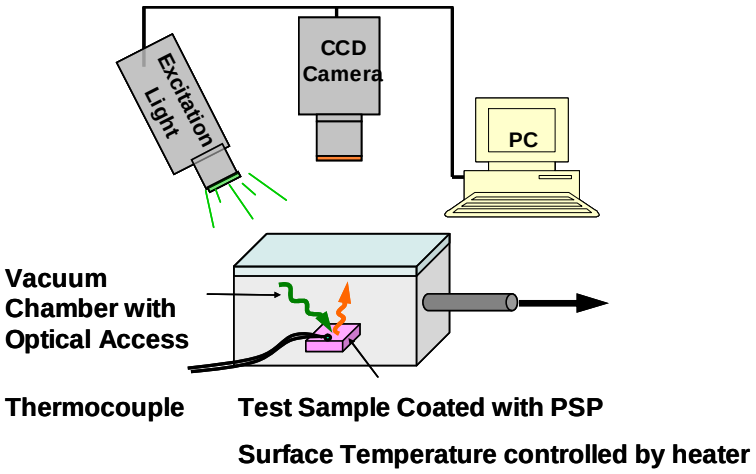

Fig. 9 PSP calibration setup

A transparent window is located over the test surface, and the CCD camera is mounted above the window. The strobe light is positioned so that maximum excitation of the PSP occurs. The camera records the emitted intensity of the PSP as gray-scale images, which are saved as TIFF files. The resulting intensity ratio can be converted to pressure ratio using a pre-determined calibration curve and can be expressed as:

$$\frac{I_{ref} - I_{black}}{I - I_{black}} = f\left(\frac{\left(P_{O_2}\right)_{air}}{\left(P_{O_2}\right)_{ref}}\right) = f\left(P_{ratio}\right) \quad (2)$$

It was observed that if the emitted light intensity at certain temperature was normalized with the reference image intensity at the same temperature, the temperature sensitivity can be minimized. Figure 10 shows the results of the calibration curve.

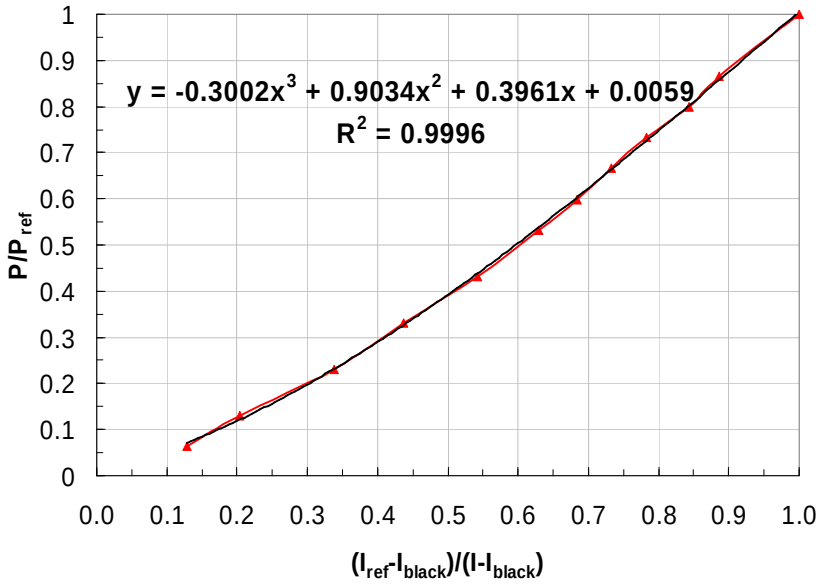

Fig. 10 Calibration curve used for the PSP method

Film Cooling Effectiveness

Four images are needed to calculate the film effectiveness: a dark image (no light, no mainstream), a reference image (with light, with mainstream), and an air injection image (with light, with mainstream, coolant is air), and a nitrogen injection image (with light, with mainstream, coolant is nitrogen). The air injection image contains information of

surface static pressure only, while the nitrogen injection image contains both the surface static pressure and the oxygen concentration information. With the calibration curve, the measured intensities are converted to the partial oxygen concentrations on the test surface.

Based on mass transfer analogy, film cooling effectiveness equation can be rewritten in terms of concentration of oxygen. Nitrogen which has nearly the same molecular weight as air, by noting the difference in partial pressure between air and nitrogen injection cases, the film cooling effectiveness can be determined using the following equation.

$$\eta = \frac{C_{mix} - C_{\infty}}{C_{N_2} - C_{\infty}} = \frac{C_{\infty} - C_{mix}}{C_{\infty}} = \frac{\left(P_{O_2}\right)_{air} - \left(P_{O_2}\right)_{mix}}{\left(P_{O_2}\right)_{air}} \tag{3}$$

Here C_{∞} is the oxygen concentration of the mainstream (near 21%) and C_{mix} is the oxygen concentration of the mainstream-coolant mixture (between 0 and 21 %). As a result, the film effectiveness will be between 0% far downstream of the coolant injection and 100% inside the hole. The mass fraction of the tracer gas in the mixture near the test surface is related to the adiabatic wall temperature for the analogous heat transfer situation.

Blowing Ratio

PSP technique is used to measure the mainstream pressure along the blade surface. Pressure taps are installed at the flow meter exit portion to measure the coolant pressure; mainstream and coolant densities can be calculated by applying ideal gas law. Blowing ratio is computed based on coolant/mainstream density, mainstream velocity, coolant volumetric flow rate and total film cooling hole area.

$$M = \frac{\rho_c \cdot V_c}{\rho_m \cdot V_m} = \frac{\left(\frac{\dot{m}}{A}\right)_c}{\rho_m \cdot V_m} = \frac{\left(\frac{\rho_c \cdot Q_c}{A_h \cdot n}\right)}{\rho_m \cdot V_m} \quad (4)$$

RESULTS AND DISCUSSIONS

Mach Number Distribution

By taking images at no coolant (blowing ratio = 0), it provided the mainstream Mach number distribution and static pressure on the test vane surface. As the exit mainstream velocity become supersonic (Mach number = 1.1 and 1.3), shockwaves take place and affect the film cooling effectiveness. Mach number distribution for three different exit Mach numbers and blowing ratio = 0 are plotted in Figure 11. By distinguishing the discontinuous velocity contour region, we can indicate the locations of potential shockwave. Dotted lines represent the approximate cooling hole row location on the suction side surface; the potential shock regions are pointed by arrows. In no coolant case, it shows that for exit Mach number = 1.1 and 1.3, shockwaves take place at near-to-trailing-edge region on the suction side surface of the test vane.

Similar Mach number distribution plots for blowing ratios of 0.5, 1.0, 1.6 and 2.0 are shown in Figures 12 to 15. Results show that, with coolant ejection, shock locates at almost the same locations for supersonic exit mainstream conditions. Due to ejected coolant mixed with mainstream air and causes complex turbulence and mixing, Mach number distribution and shockwaves' location are different than no coolant case (M = 0).

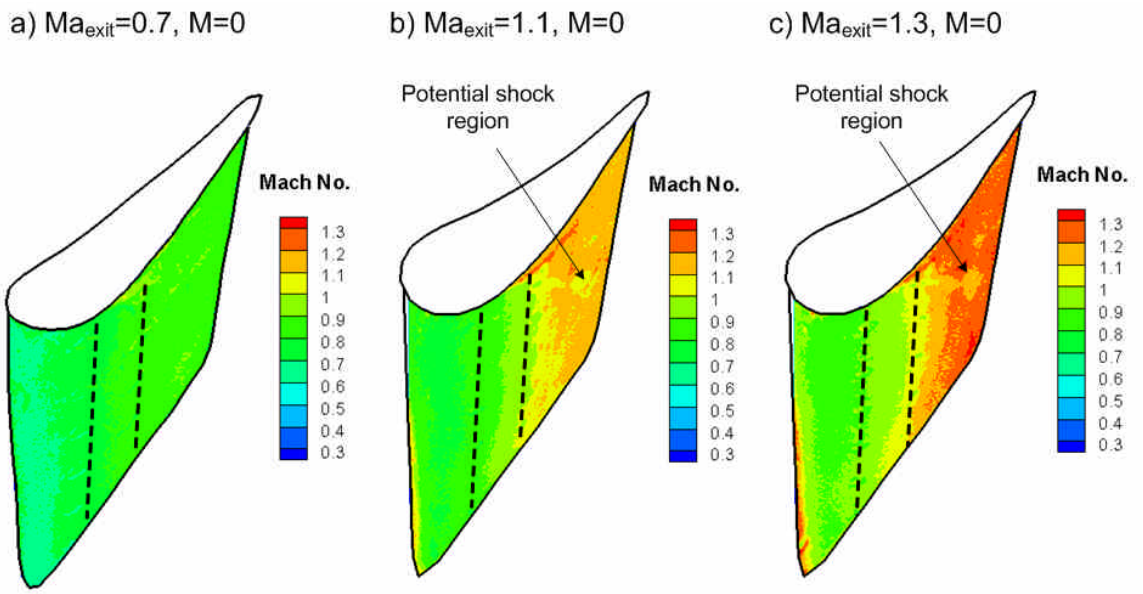

Fig. 11 Mach number distribution contour plots for blowing ratio = 0 and exit Mach numbers of (a) 0.7, (b) 1.1, and (c) 1.3

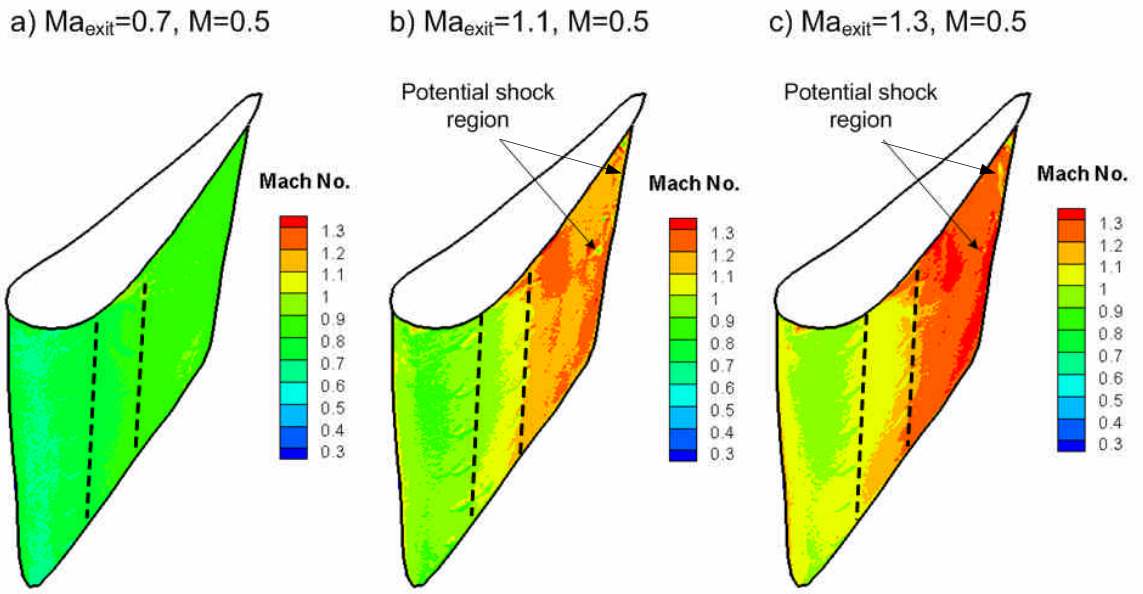

Fig. 12 Mach number distribution contour plots for blowing ratio = 0.5 and exit Mach numbers of (a) 0.7, (b) 1.1, and (c) 1.3

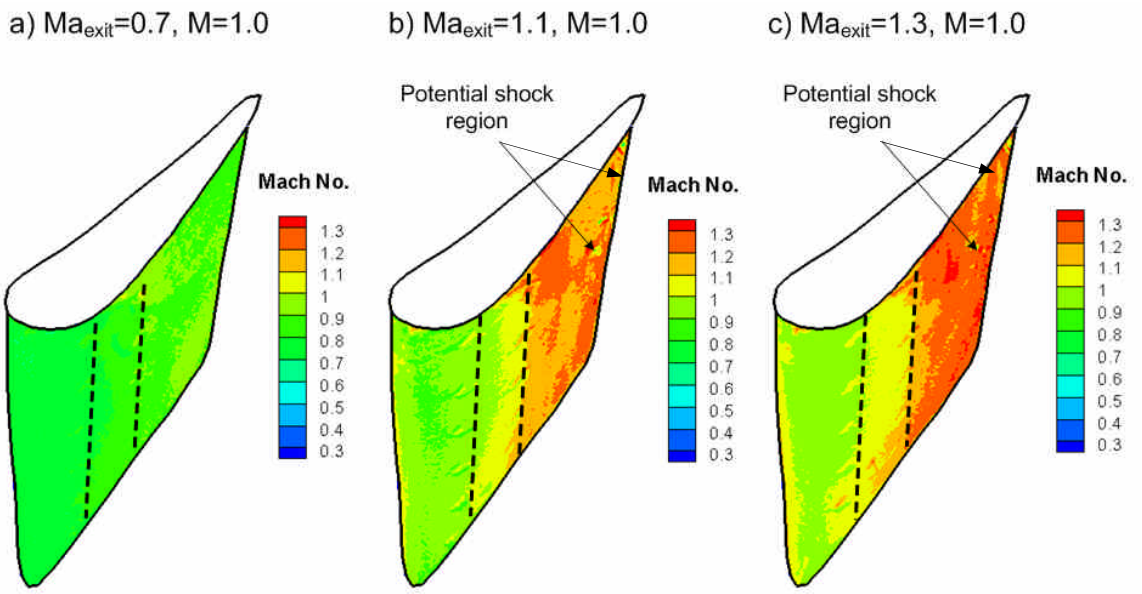

Fig. 13 Mach number distribution contour plots for blowing ratio = 1.0 and exit Mach numbers of (a) 0.7, (b) 1.1, and (c) 1.3

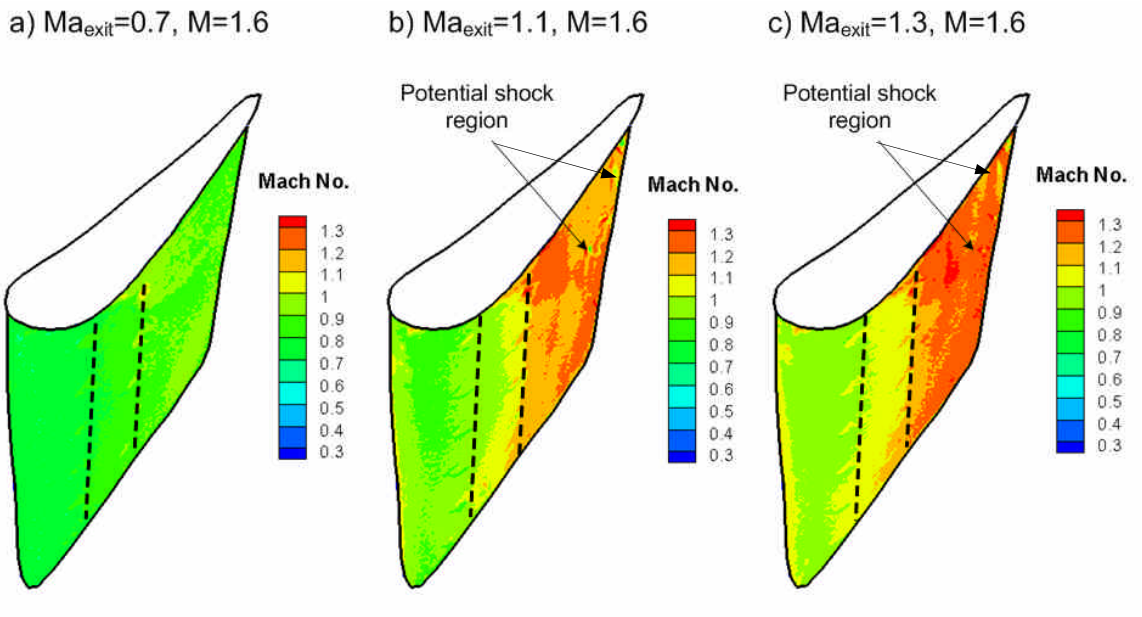

Fig. 14 Mach number distribution contour plots for blowing ratio = 1.6 and exit Mach numbers of (a) 0.7, (b) 1.1, and (c) 1.3

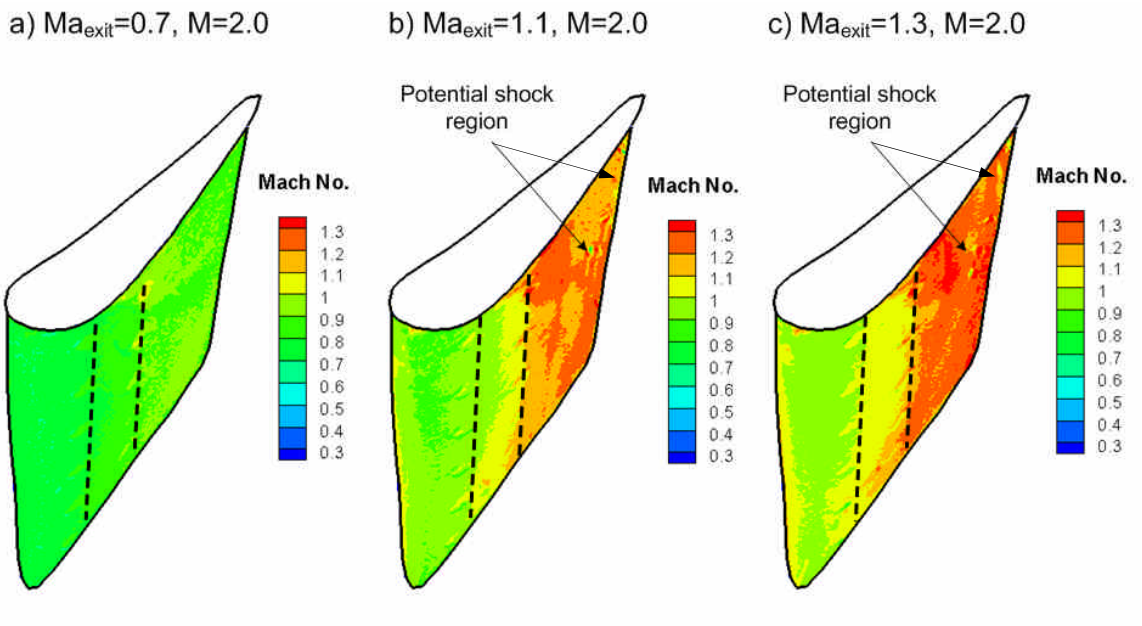

Fig. 15 Mach number distribution contour plots for blowing ratio = 2.0 and exit Mach numbers of (a) 0.7, (b) 1.1, and (c) 1.3

Film Cooling Effectiveness

The pressure sensitive paint was uniformly sprayed onto the test surface. With the calibration curve, the measured intensities are converted to the partial oxygen concentrations on the test surface; moreover, film cooling effectiveness can be calculated. The camera angle shows in Figure 16 was found to give us the best view of the vane surface. However, one hole from suction side row 1 and two holes from suction side row 2are beyond the field of view of the camera.

3D film cooling effectiveness contour plots are shown in Figures 17 to 20. As the result, for subsonic exit condition, blowing ratio = 1.0 provides the greatest film cooling effectiveness; for supersonic exit velocities, the optimum blowing ratio is about 1.6. When the blowing ratio exceeds the critical value, the trace left from the coolant becomes narrower resulting in less coverage and lower effectiveness.

Before it reaches the optimum blowing ratio, the effectiveness increases with blowing ratio due to coolant supply increases; after reaching the optimum value, effectiveness decreases with blow ratio because the increase of momentum as the blowing ratio increases, and causes the coolant jet liftoff. Higher momentum promotes more mixing between the mainstream and coolant flows. The coolant detaches from the surface immediately downstream of the holes exposing the surface to the mainstream flow and decreasing the effectiveness.

As the coolant is separated from the surface, it is also pushed by the mainstream flow back to the surface. This reattachment back to the surface results in higher local effectiveness as the coolant impinges back onto the surface. For exit Mach number = 1.1 and 1.3, reattachment effects can be seen from the leading edge portion as the blowing ration increases form 1.0 to 1.6, where the effectiveness suddenly increases downstream of the leading edge film cooling holes. At low exit Mach number, the mainstream is not strong enough to blow the leading edge coolant jet from pressure side to suction side. Therefore, there is no coolant trace can be seen at the leading edge portion.

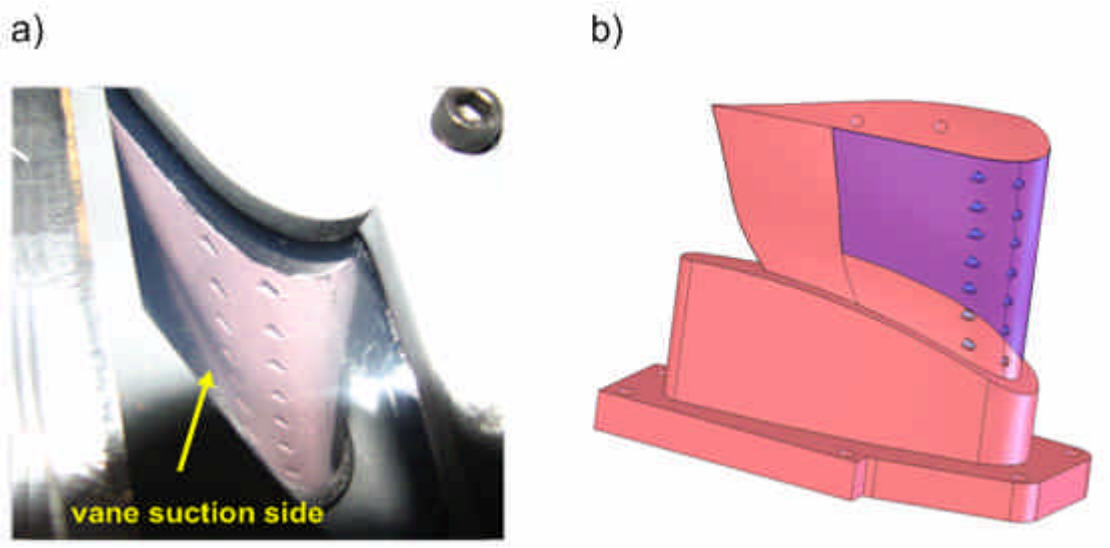

Fig. 16 (a) Actual camera view for the test vane surface, and (b) Shaded area is the field of camera view

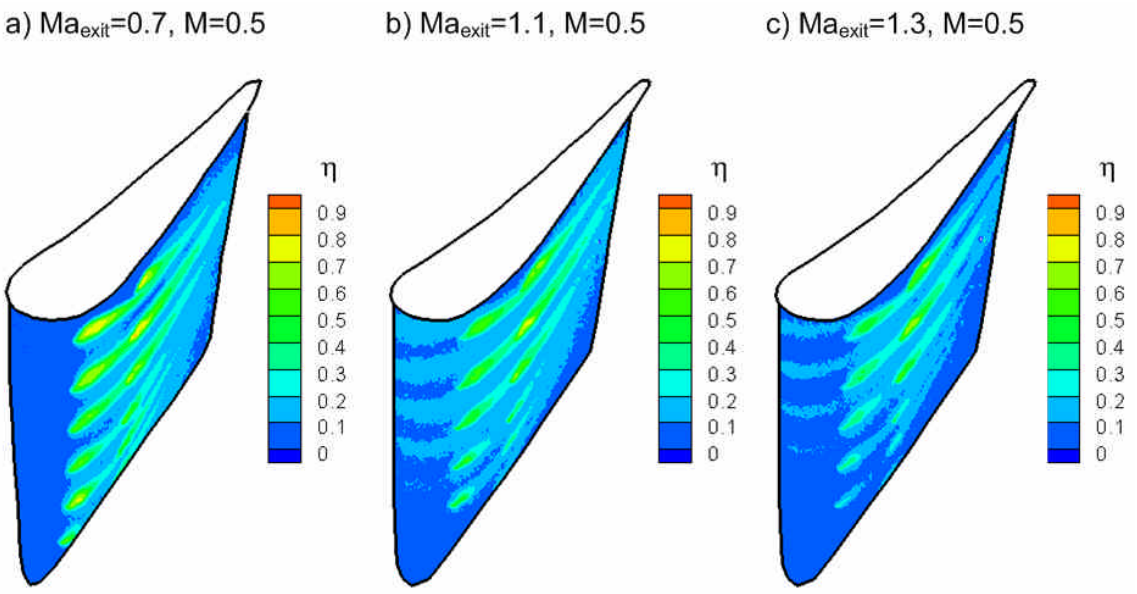

Fig. 17 Cooling effectiveness distribution contour plots for blowing ratio = 0.5 and exit Mach numbers of (a) 0.7, (b) 1.1, and (c) 1.3

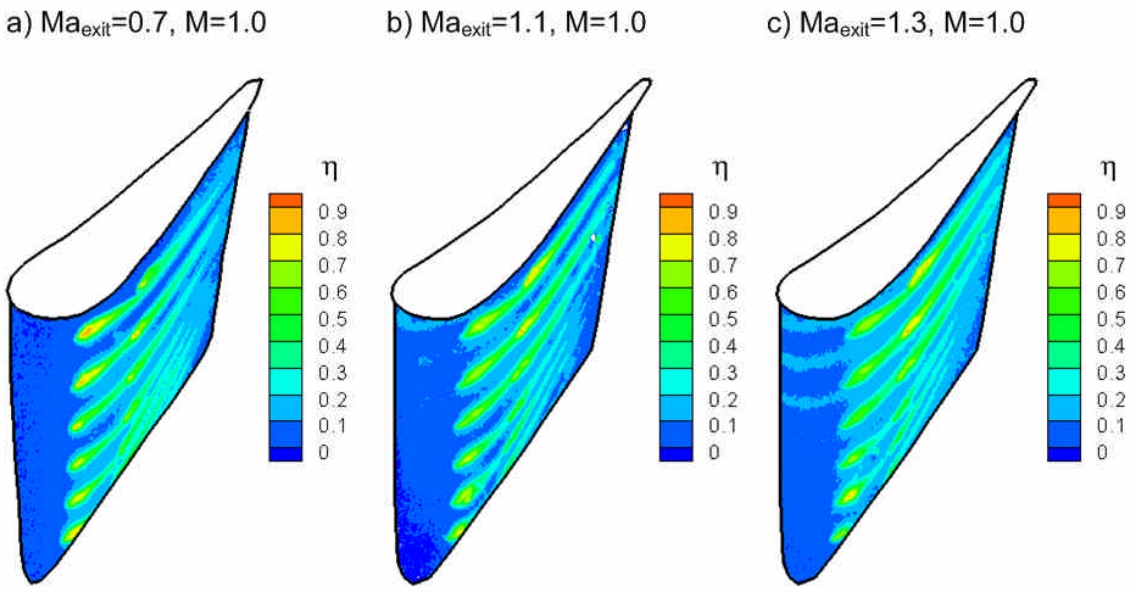

Fig. 18 Cooling effectiveness distribution contour plots for blowing ratio = 1.0 and exit Mach numbers of (a) 0.7, (b) 1.1, and (c) 1.3

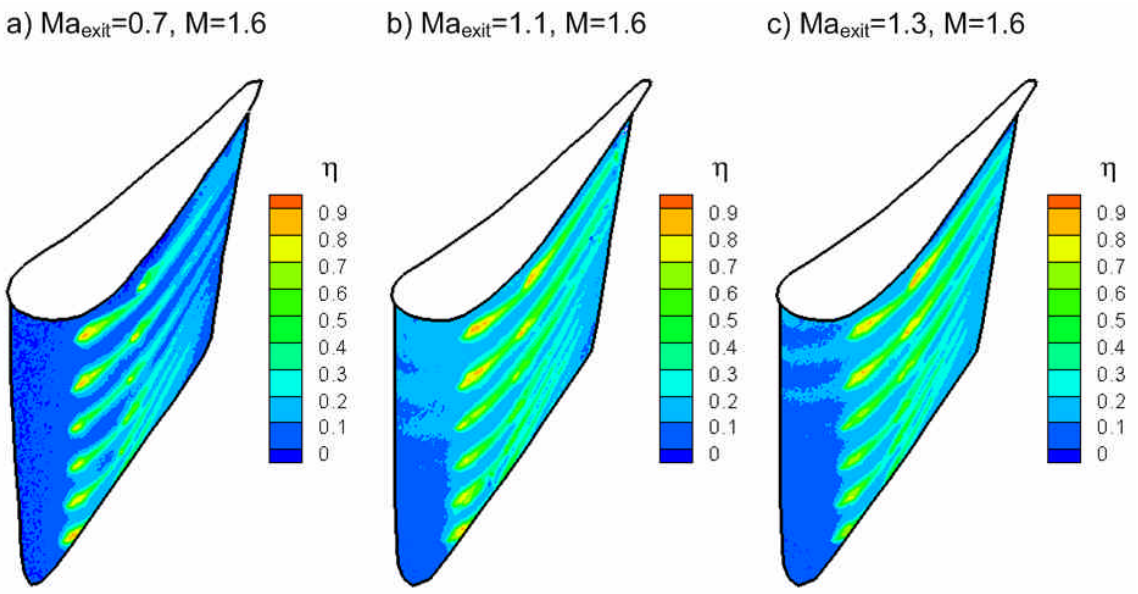

Fig. 19 Cooling effectiveness distribution contour plots for blowing ratio = 1.6 and exit Mach numbers of (a) 0.7, (b) 1.1, and (c) 1.3

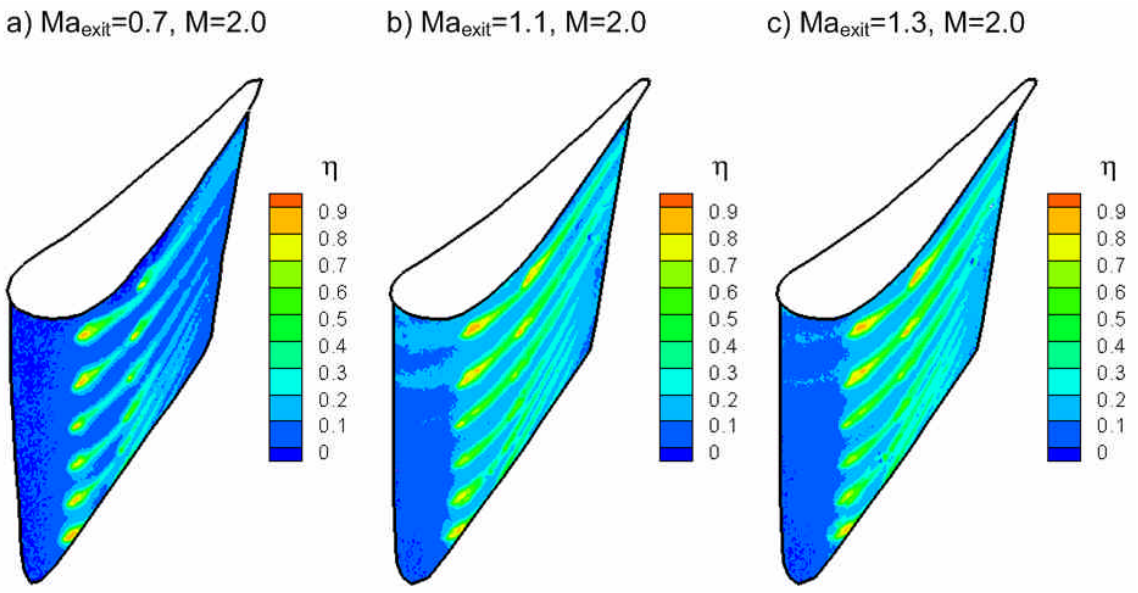

Fig. 20 Cooling effectiveness distribution contour plots for blowing ratio = 2.0 and exit Mach numbers of (a) 0.7, (b) 1.1, and (c) 1.3

In order to have a better view of shock effects on film cooling trace, magnified images, focusing on the trailing edge portion are provided. Figure 21 shows the relative magnified region on the test vane surface. Magnified Mach number and corresponding cooling effectiveness distribution are shown in Figures 22 to 29, dotted line represents the approximate cooling hole row location on the suction side surface and the potential shock locations have been circled.

By comparing the Mach number and effectiveness distributions, it can be seen that shocks take place at almost the same position in each case. The locations are at the training edge and on the tail of the coolant trace. However, the shock does not change the shape or direction of film cooling trace, because the film trace has died out before shock occurs.

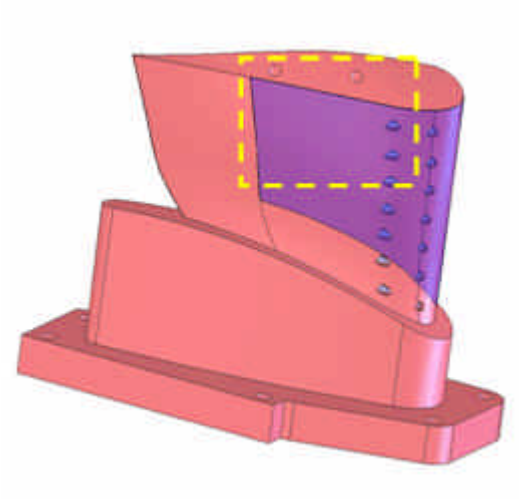

Fig. 21 Yellow-square area is the magnified region

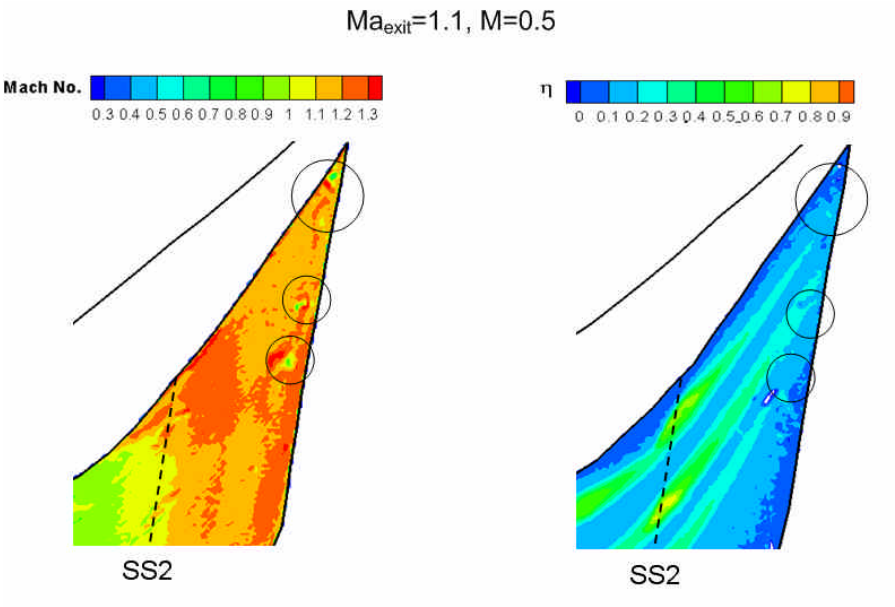

Fig. 22 Magnified Mach number and effectiveness distribution for exit Mach numbers of 1.1 and blowing ratio = 0.5

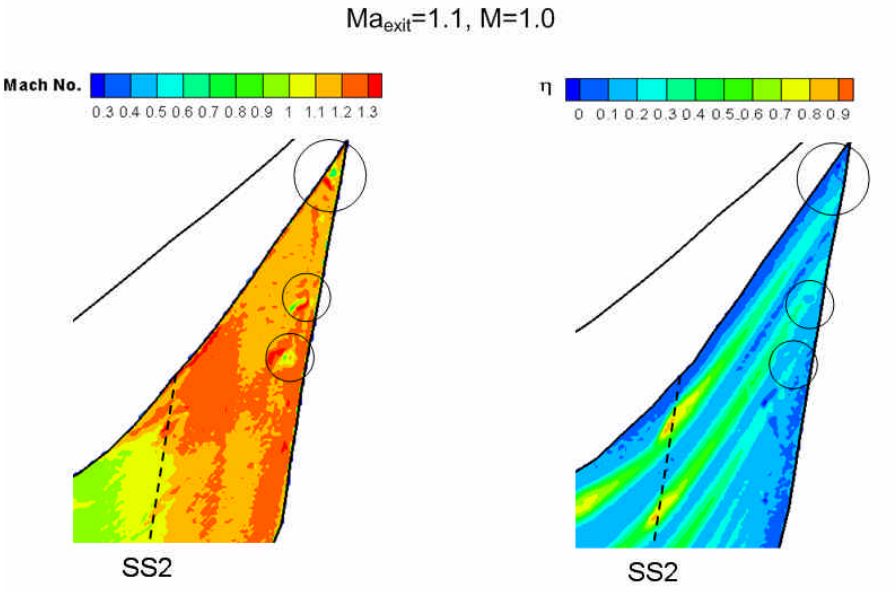

Fig. 23 Magnified Mach number and effectiveness distribution for exit Mach numbers of 1.1 and blowing ratio = 1.0

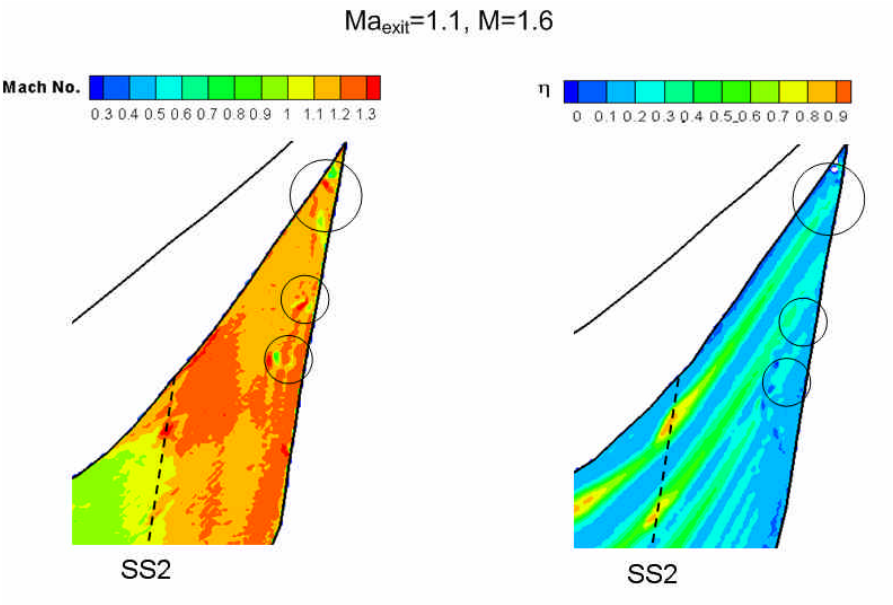

Fig. 24 Magnified Mach number and effectiveness distribution for exit Mach numbers of 1.1 and blowing ratio = 1.6

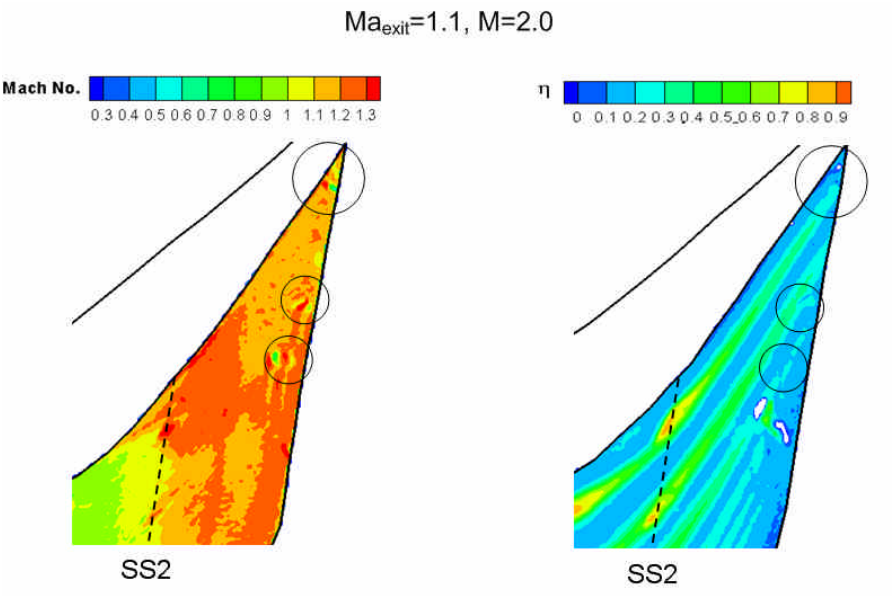

Fig. 25 Magnified Mach number and effectiveness distribution for exit Mach numbers of 1.1 and blowing ratio = 2.0

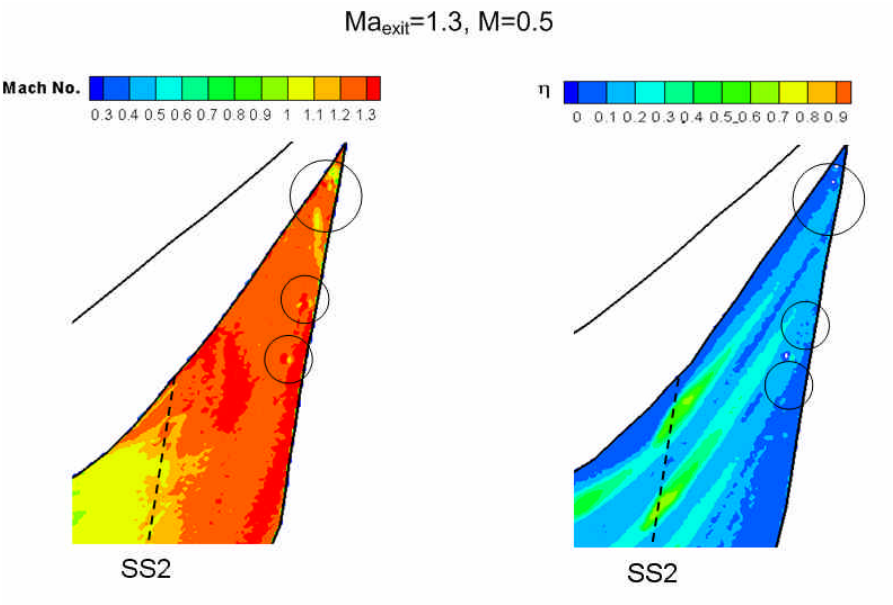

Fig. 26 Magnified Mach number and effectiveness distribution for exit Mach numbers of 1.3 and blowing ratio = 0.5

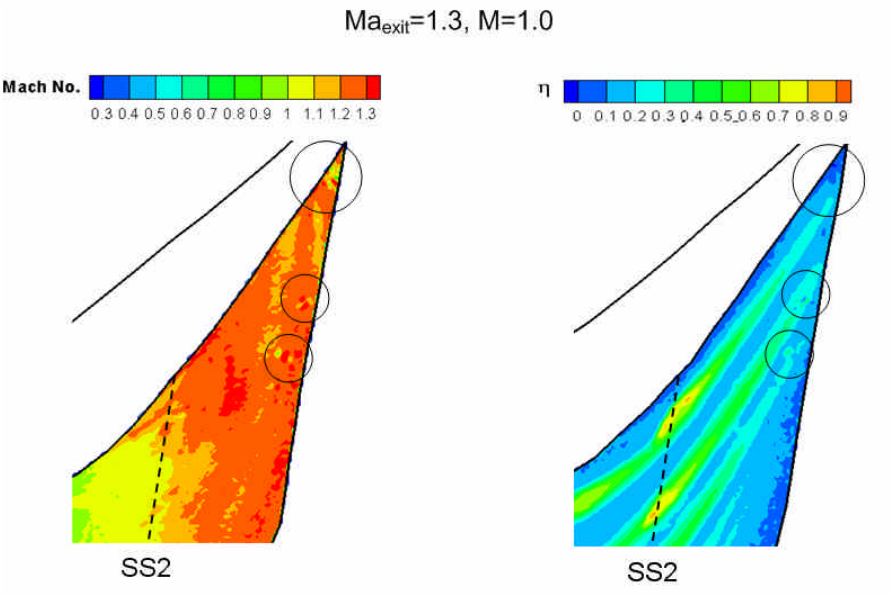

Fig. 27 Magnified Mach number and effectiveness distribution for exit Mach numbers of 1.3 and blowing ratio = 1.0

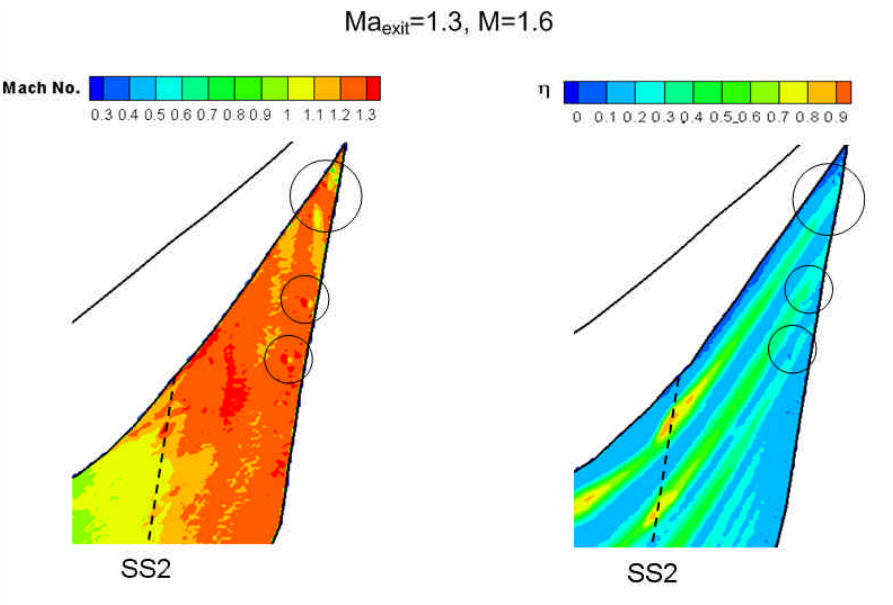

Fig. 28 Magnified Mach number and effectiveness distribution for exit Mach numbers of 1.3 and blowing ratio = 1.6

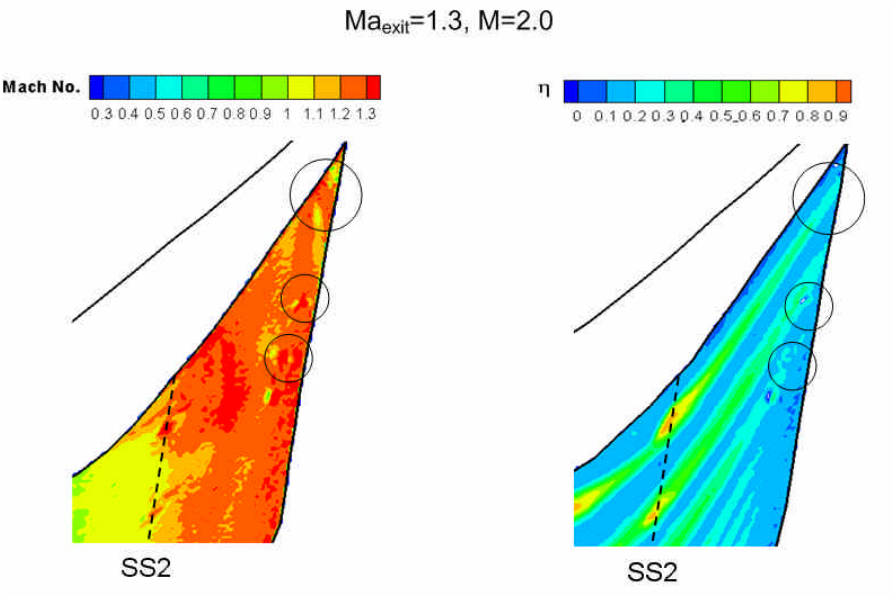

Fig. 29 Magnified Mach number and effectiveness distribution for exit Mach numbers of 1.3 and blowing ratio = 2.0

Figures 30 to 41 show the 2D contour plots of film cooling effectiveness, this provides more clear and better pictures for the coolant trace and the effectiveness level. For subsonic condition, M = 1.0 has the optimum effectiveness. For supersonic condition, M = 1.6 provides the optimum cooling effectiveness. Further increase of blowing ratio causes the narrower traced and resulting in less coverage and lower effectiveness. This is due to the increase of momentum as the blowing ratio increases, and causes the coolant jet liftoff. The inclined hub portion of test vane performs as a nozzle and redirects the mainstream flow; due to horseshoes vortices and secondary flow effects, the film cooling trace near the hub has been bended upward.

Figures 42 to 53 show the averaged effectiveness for the four blowing ratios and three mainstream velocities. The effectiveness data is plotted for non-dimensional distance of x/MS – the downstream distance (x) divided by the blowing ratio (M) and equivalent slot width (S). This parameter is used to try to correlate the data for all blowing ratios onto one curve. The plots are given for 50% and 91% of span surface length. The 50% span pass through the middle film cooling hole from row 1 and row 2; the 91% span pass through the first film cooling hole from the top of row 1 and row 2. Two major peaks on 91% span indicate two film cooling holes from row 1 and row 2; 50% span have two major peaks and multiple small peaks, small peaks are due to the bended coolant trace near the hub portion.

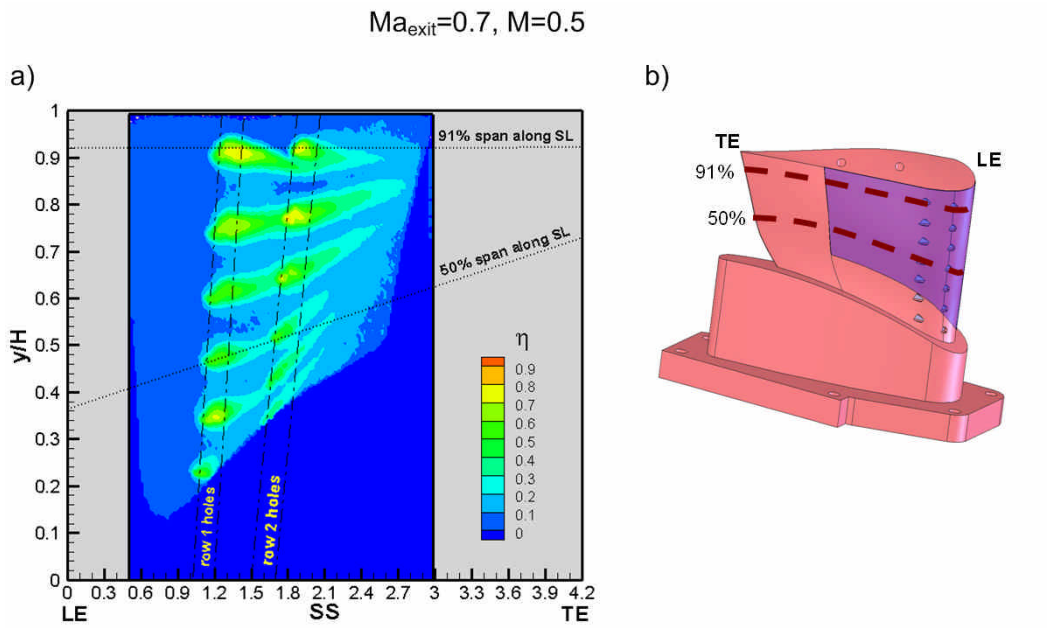

Fig. 30 a) 2D effectiveness distribution along surface length for and exit Mach numbers of 0.7 and blowing ratio = 0.5, b) corresponding span position on the test vane surface

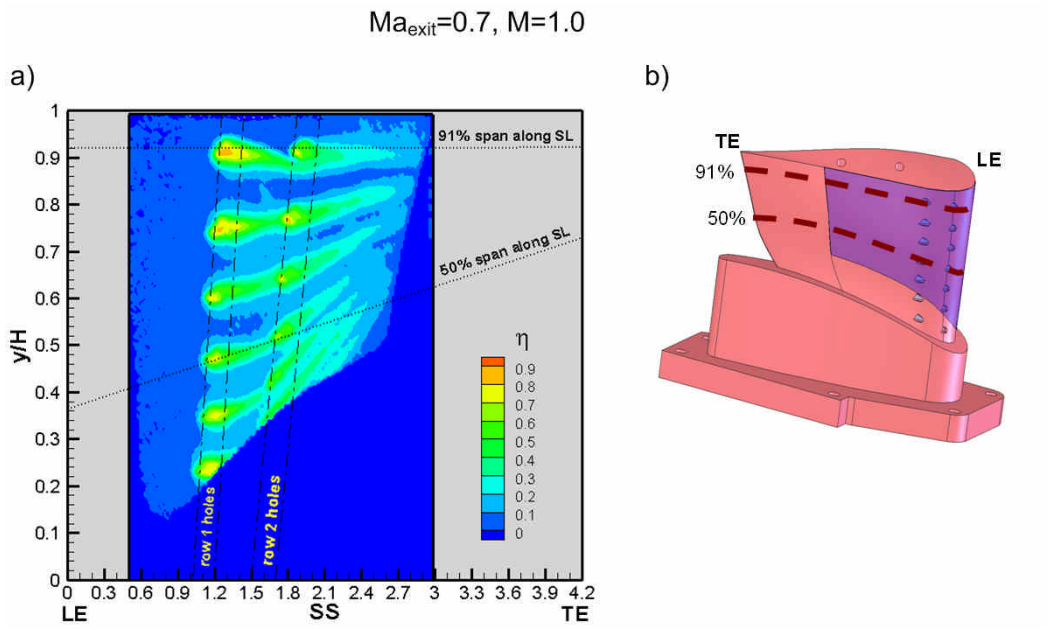

Fig. 31 a) 2D effectiveness distribution along surface length for and exit Mach numbers of 0.7 and blowing ratio = 1.0, b) corresponding span position on the test vane surface

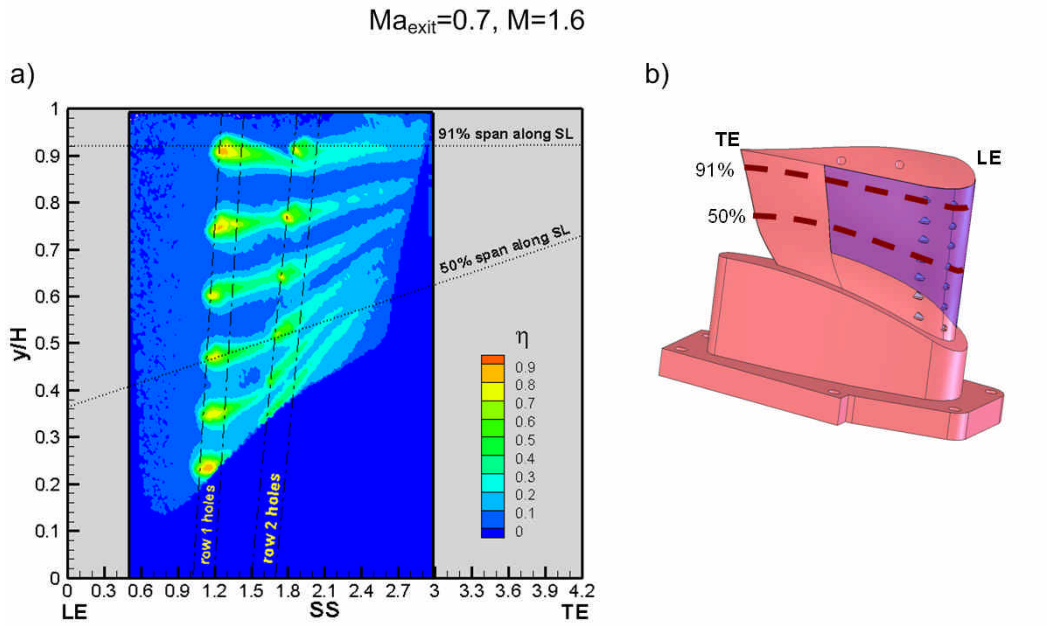

Fig. 32 a) 2D effectiveness distribution along surface length for and exit Mach numbers of 0.7 and blowing ratio = 1.6, b) corresponding span position on the test vane surface

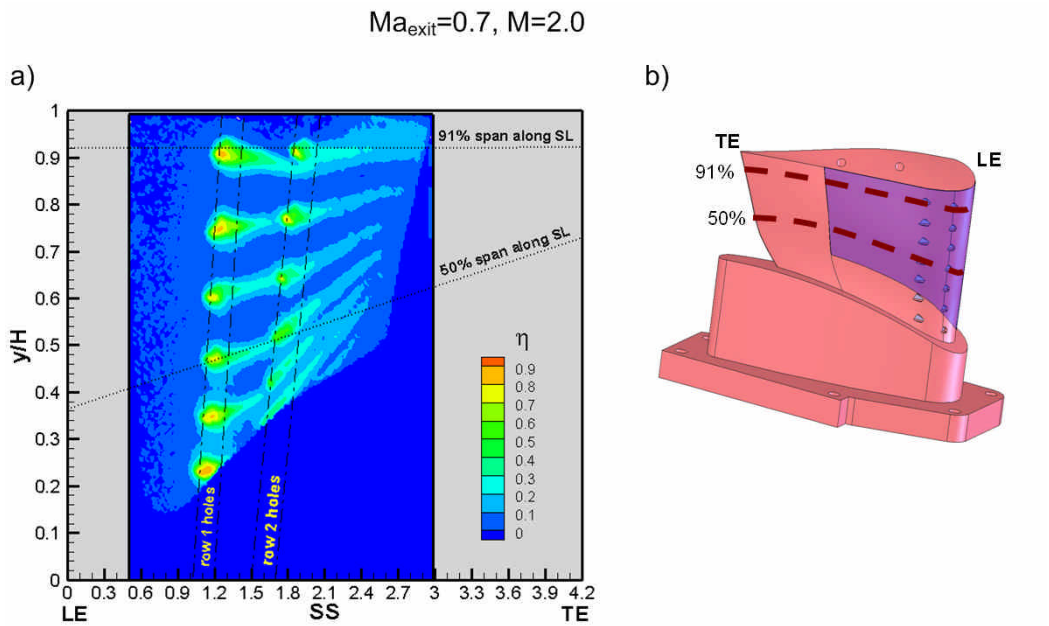

Fig. 33 a) 2D effectiveness distribution along surface length for and exit Mach numbers of 0.7 and blowing ratio = 2.0, b) corresponding span position on the test vane surface

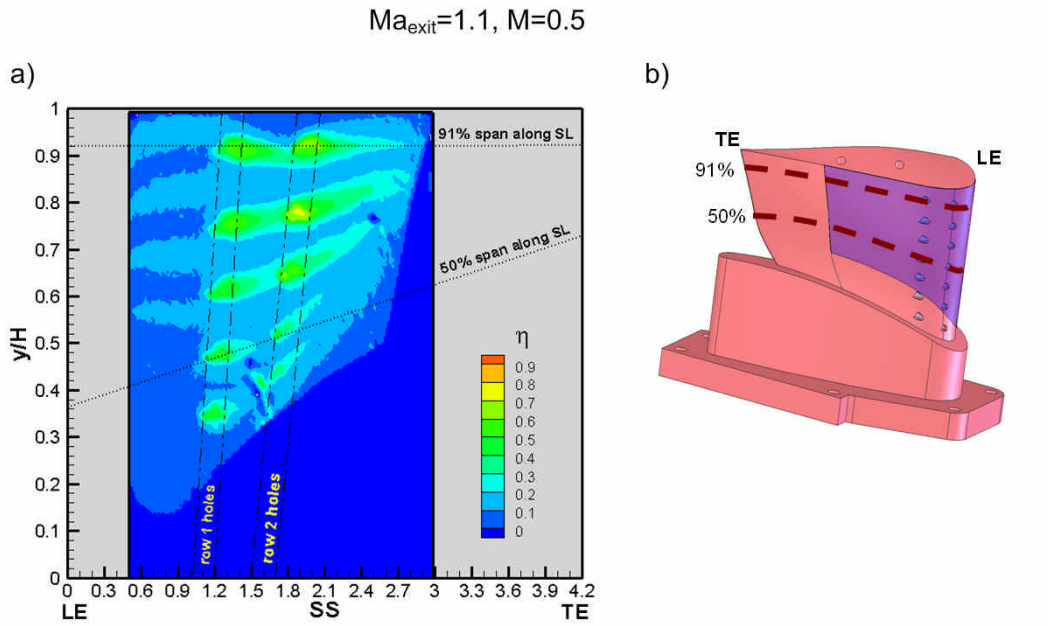

Fig. 34 a) 2D effectiveness distribution along surface length for and exit Mach numbers of 1.1 and blowing ratio = 0.5, b) corresponding span position on the test vane surface

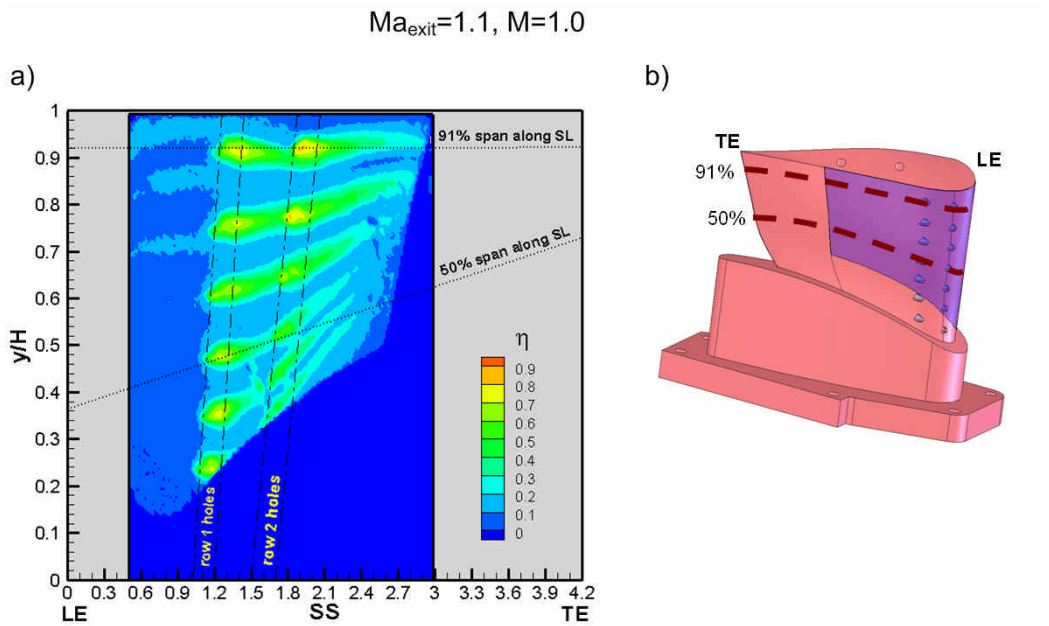

Fig. 35 a) 2D effectiveness distribution along surface length for and exit Mach numbers of 1.1 and blowing ratio = 1.0, b) corresponding span position on the test vane surface

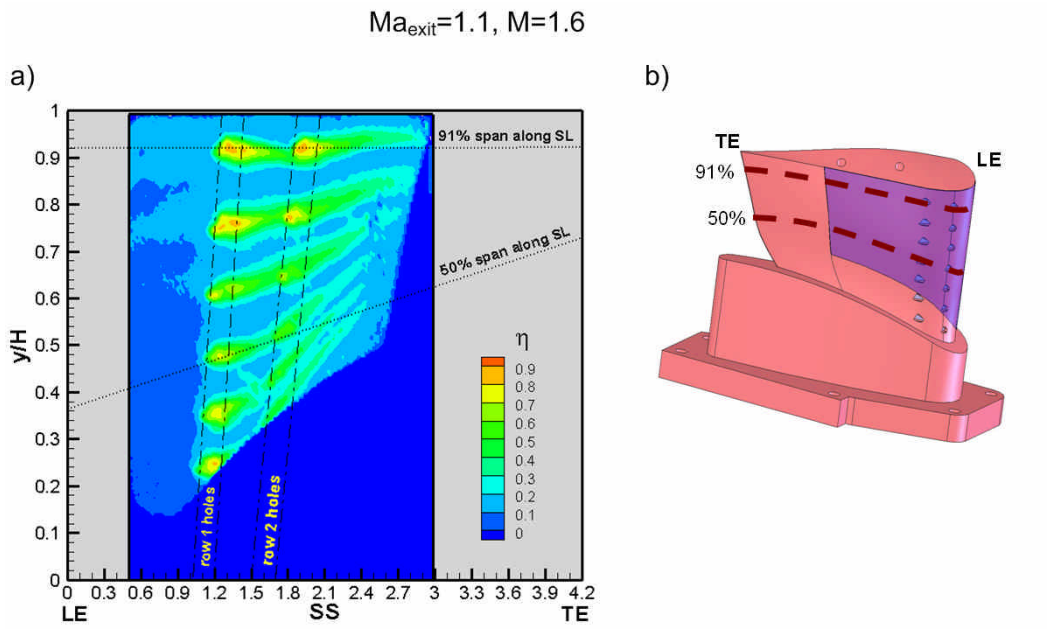

Fig. 36 a) 2D effectiveness distribution along surface length for and exit Mach numbers of 1.1 and blowing ratio = 1.6, b) corresponding span position on the test vane surface

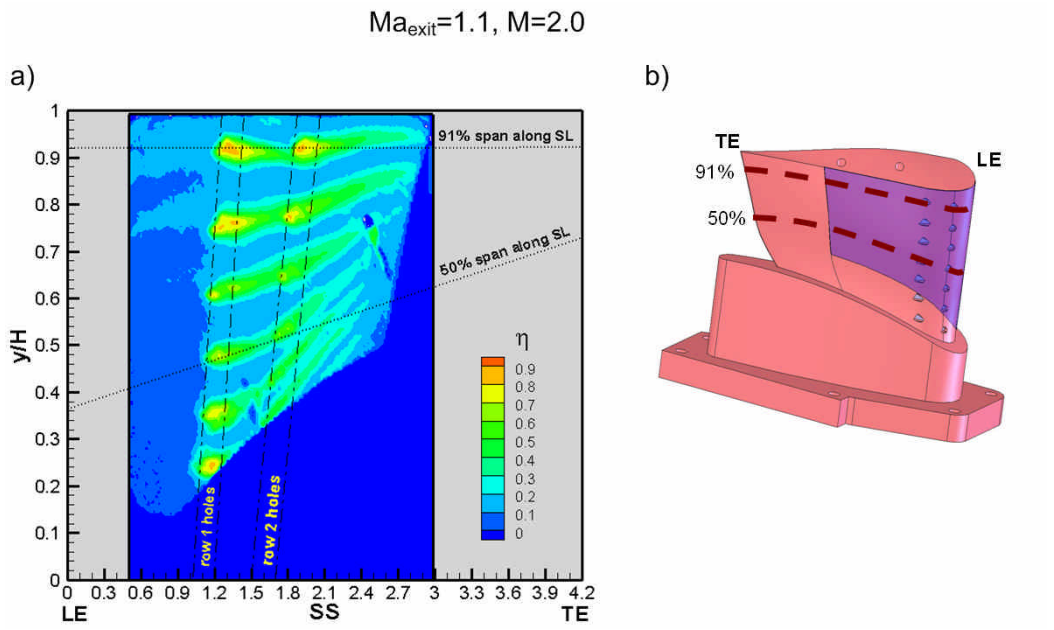

Fig. 37 a) 2D effectiveness distribution along surface length for and exit Mach numbers of 1.1 and blowing ratio = 2.0, b) corresponding span position on the test vane surface

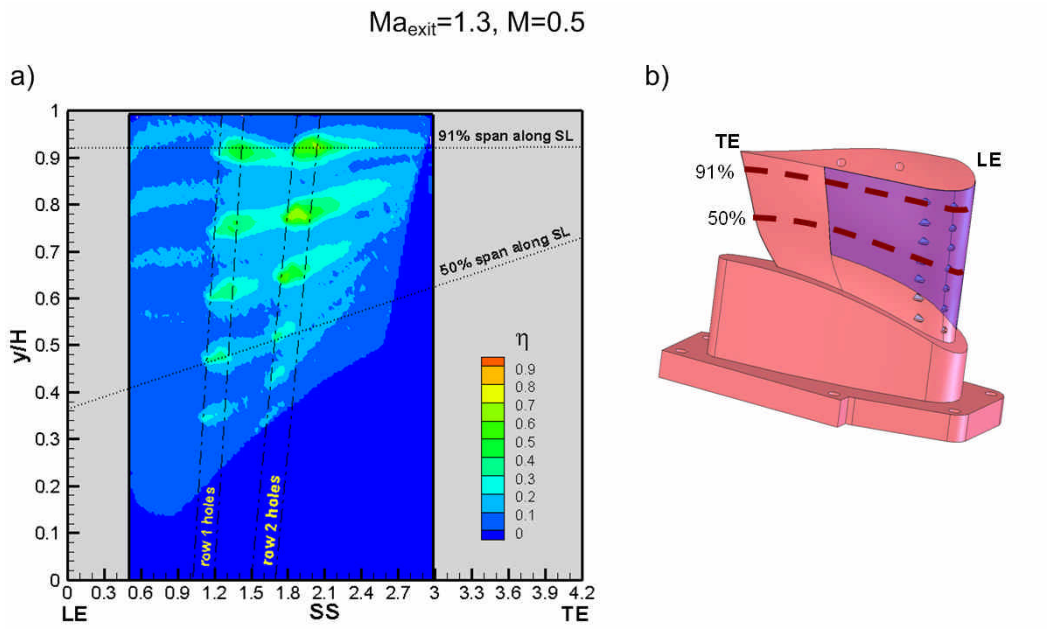

Fig. 38 a) 2D effectiveness distribution along surface length for and exit Mach numbers of 1.3 and blowing ratio = 0.5, b) corresponding span position on the test vane surface

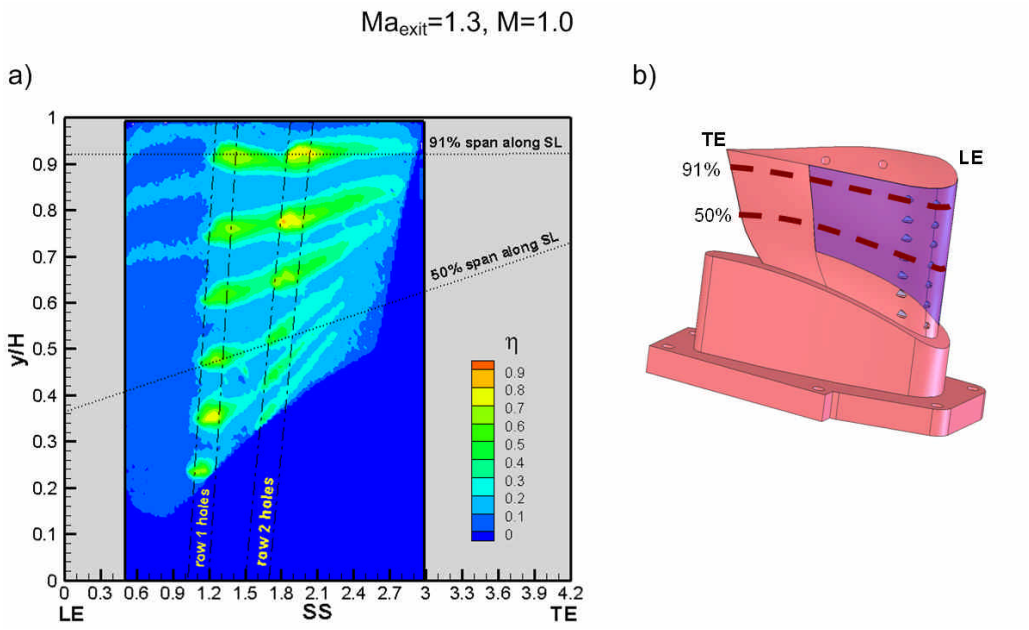

Fig. 39 a) 2D effectiveness distribution along surface length for and exit Mach numbers of 1.3 and blowing ratio = 1.0, b) corresponding span position on the test vane surface

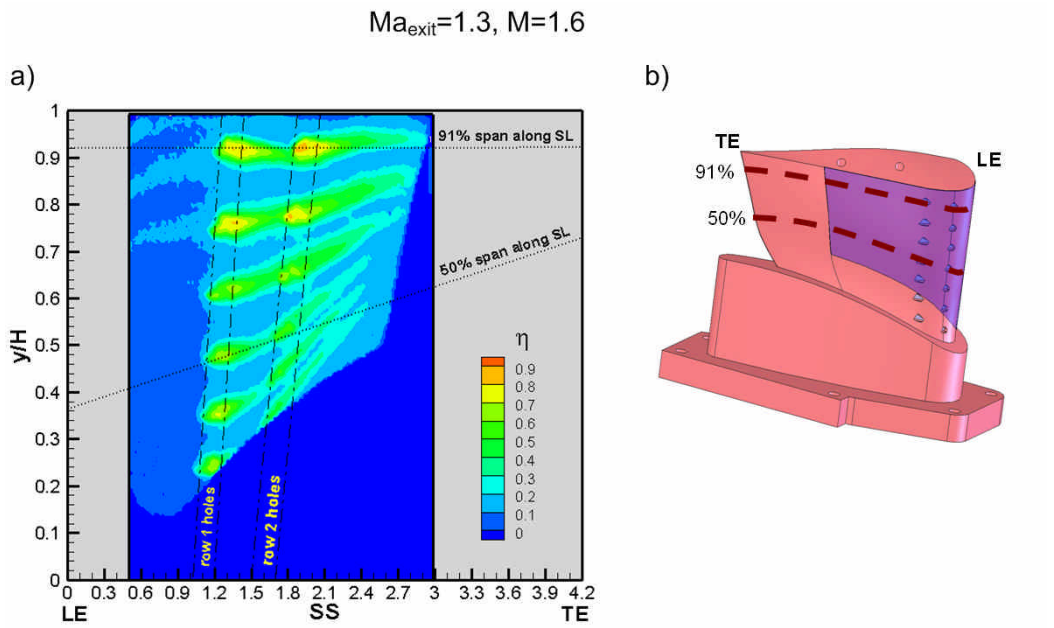

Fig. 40 a) 2D effectiveness distribution along surface length for and exit Mach numbers of 1.3 and blowing ratio = 1.6, b) corresponding span position on the test vane surface

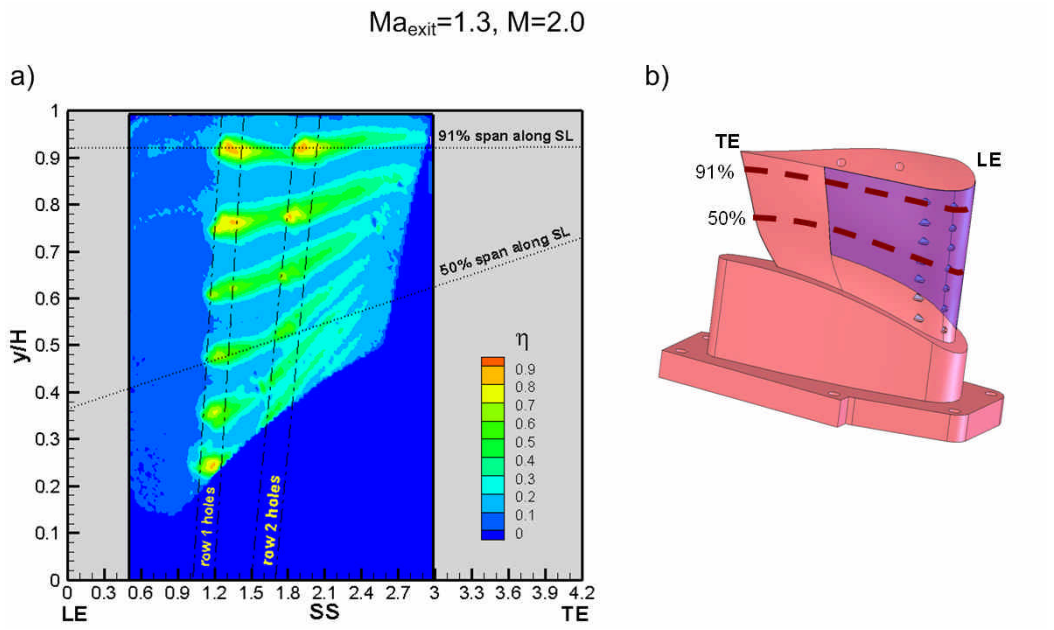

Fig. 41 a) 2D effectiveness distribution along surface length for and exit Mach numbers of 1.3 and blowing ratio = 2.0, b) corresponding span position on the test vane surface

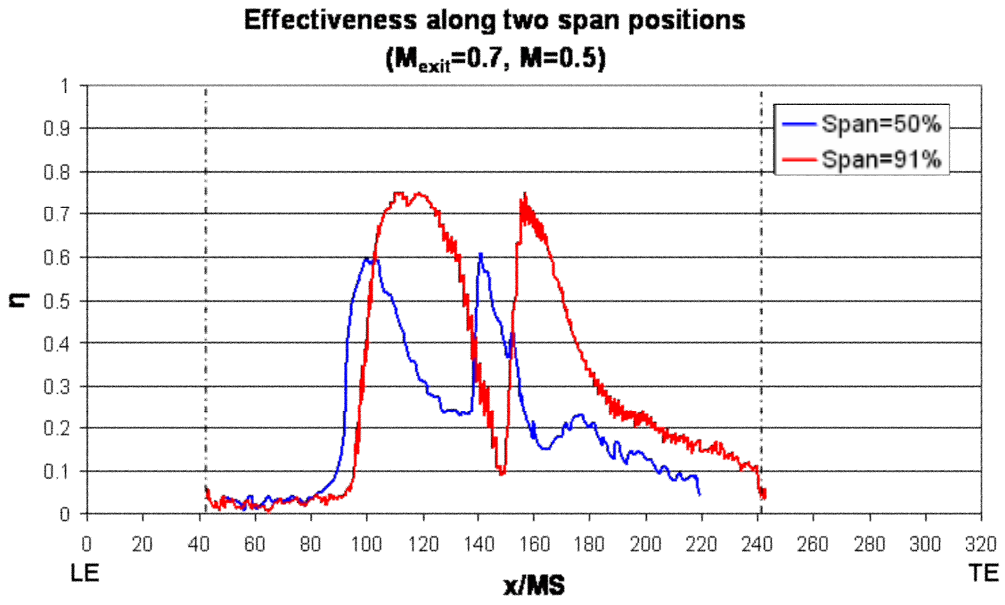

Fig. 42 Effectiveness along two spans position for and exit Mach numbers of 0.7 and blowing ratio = 0.5

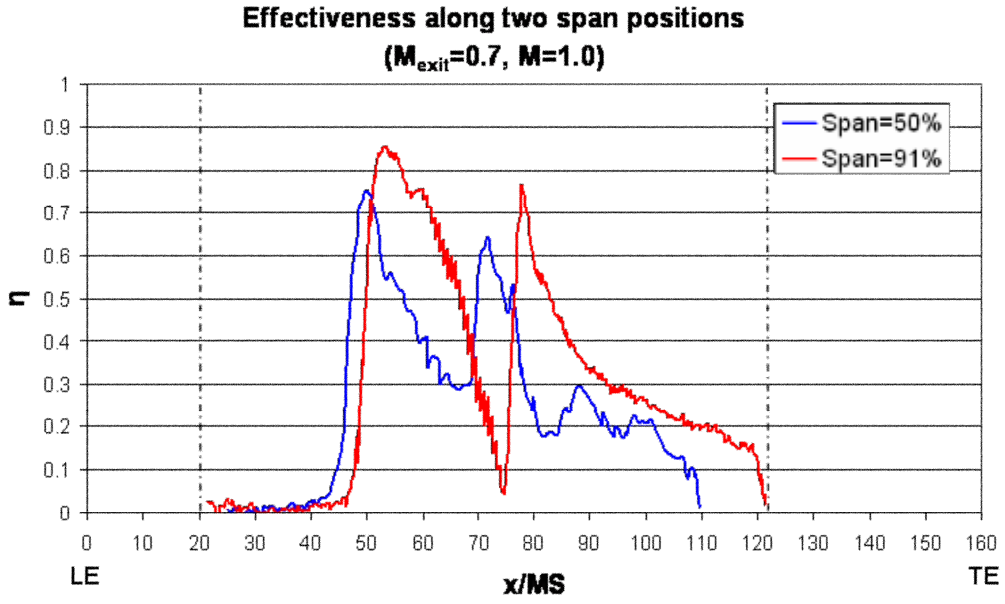

Fig. 43 Effectiveness along two spans position for and exit Mach numbers of 0.7 and blowing ratio = 1.0

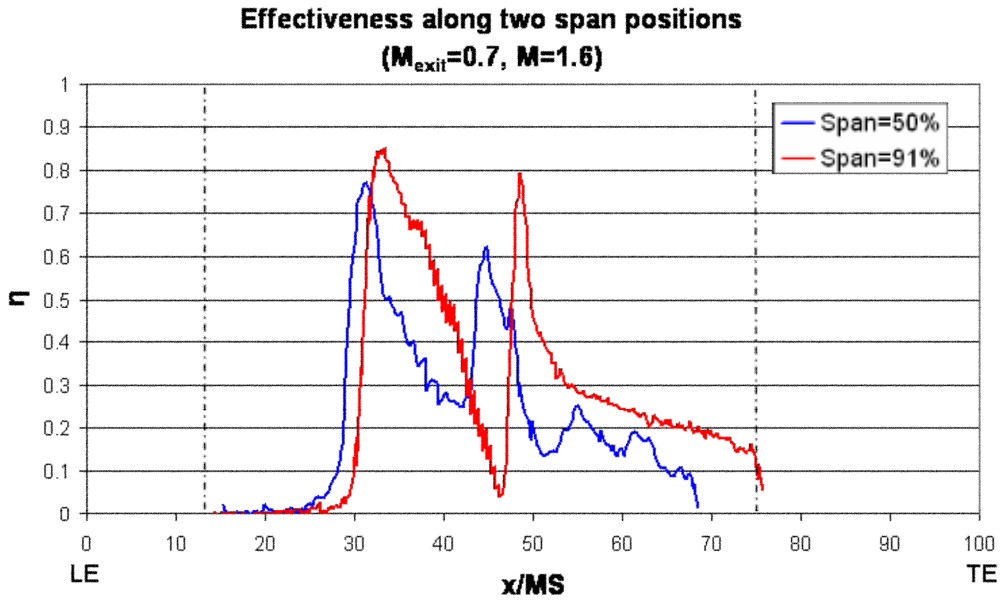

Fig. 44 Effectiveness along two spans position for and exit Mach numbers of 0.7 and blowing ratio = 1.6

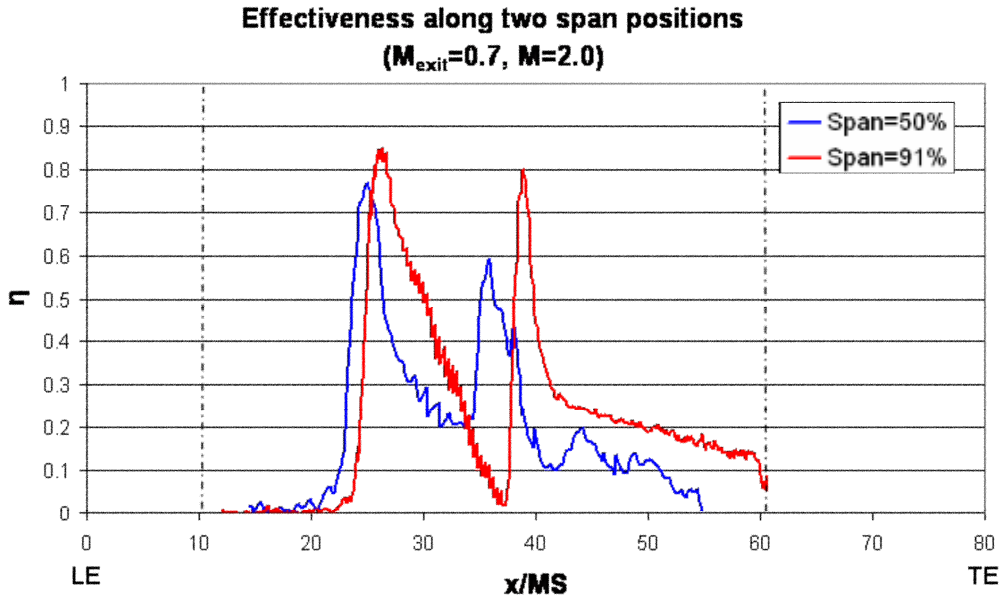

Fig. 45 Effectiveness along two spans position for and exit Mach numbers of 0.7 and blowing ratio = 2.0

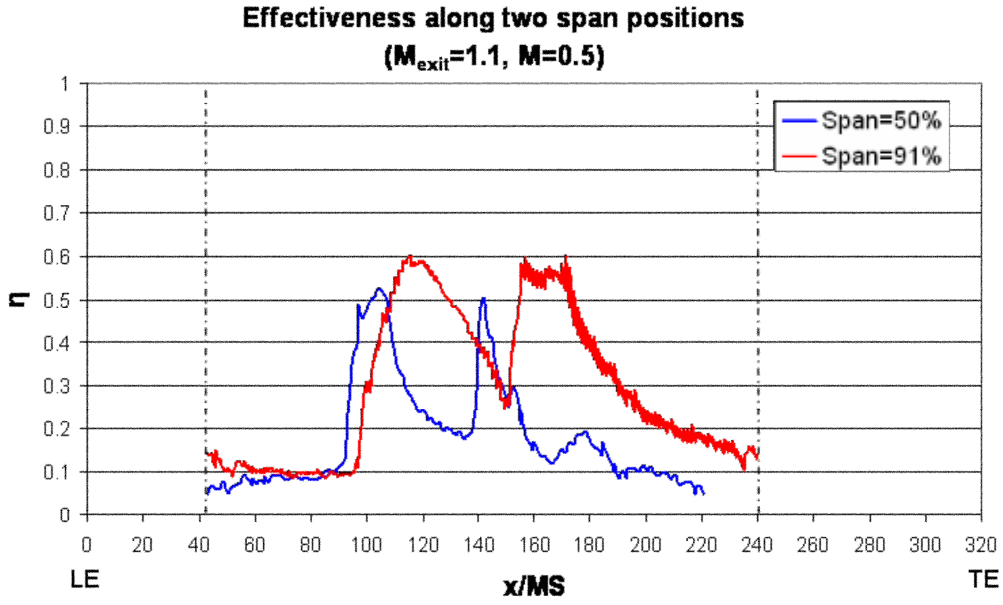

Fig. 46 Effectiveness along two spans position for and exit Mach numbers of 1.1 and blowing ratio = 0.5

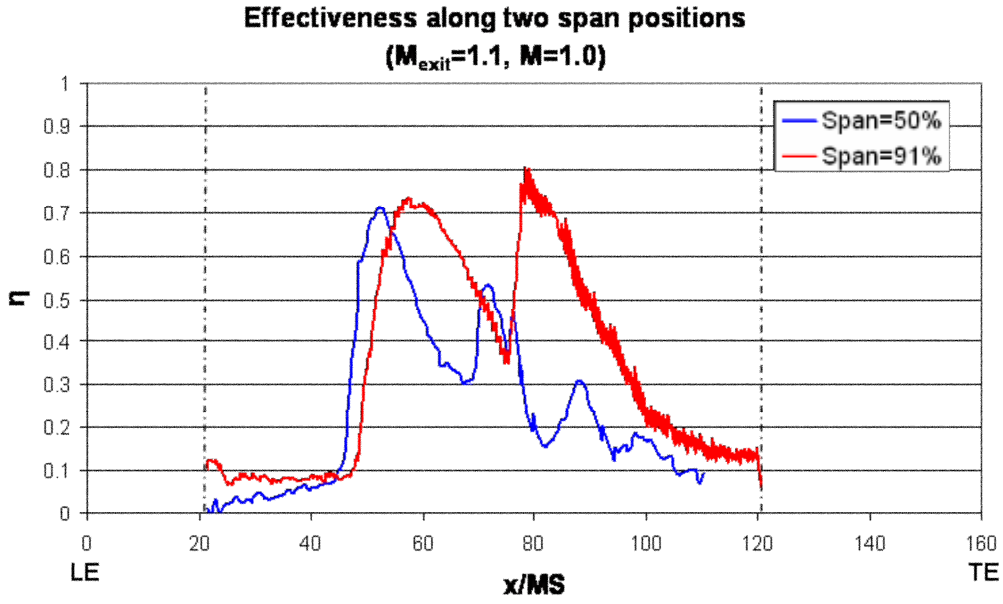

Fig. 47 Effectiveness along two spans position for and exit Mach numbers of 1.1 and blowing ratio = 1.0

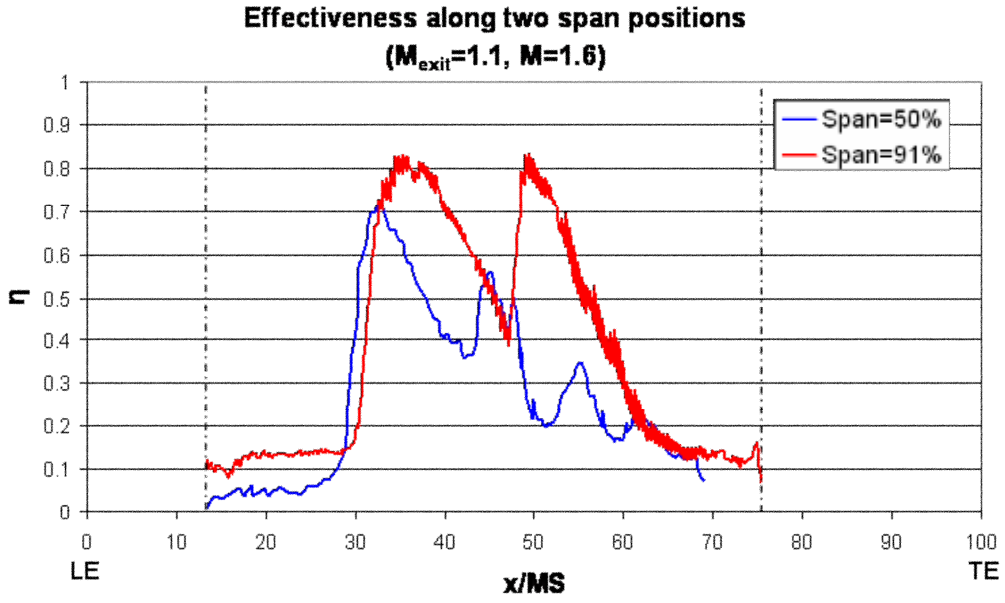

Fig. 48 Effectiveness along two spans position for and exit Mach numbers of 1.1 and blowing ratio = 1.6

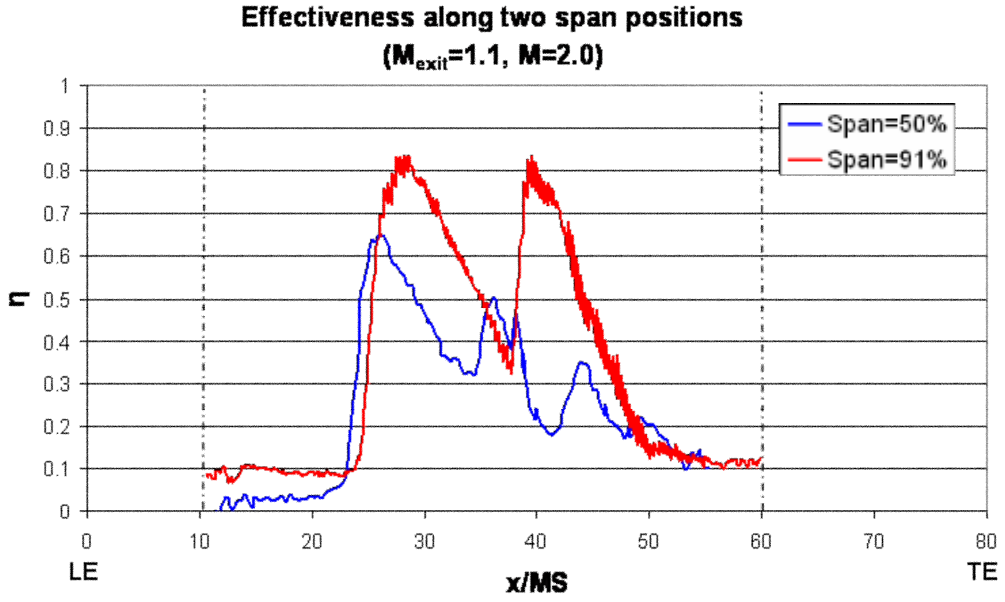

Fig. 49 Effectiveness along two spans position for and exit Mach numbers of 1.1 and blowing ratio = 2.0

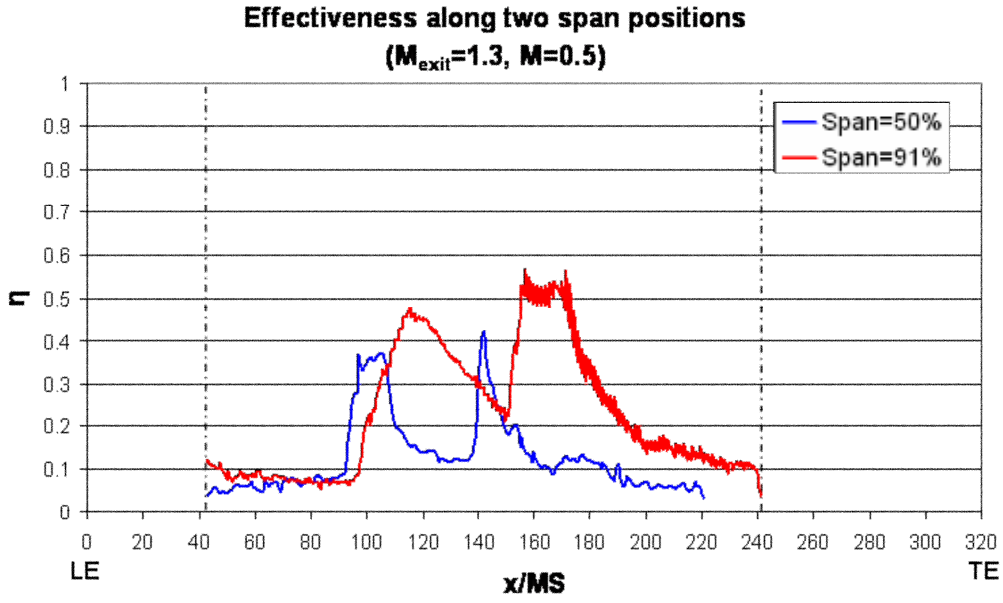

Fig. 50 Effectiveness along two spans position for and exit Mach numbers of 1.3 and blowing ratio = 0.5

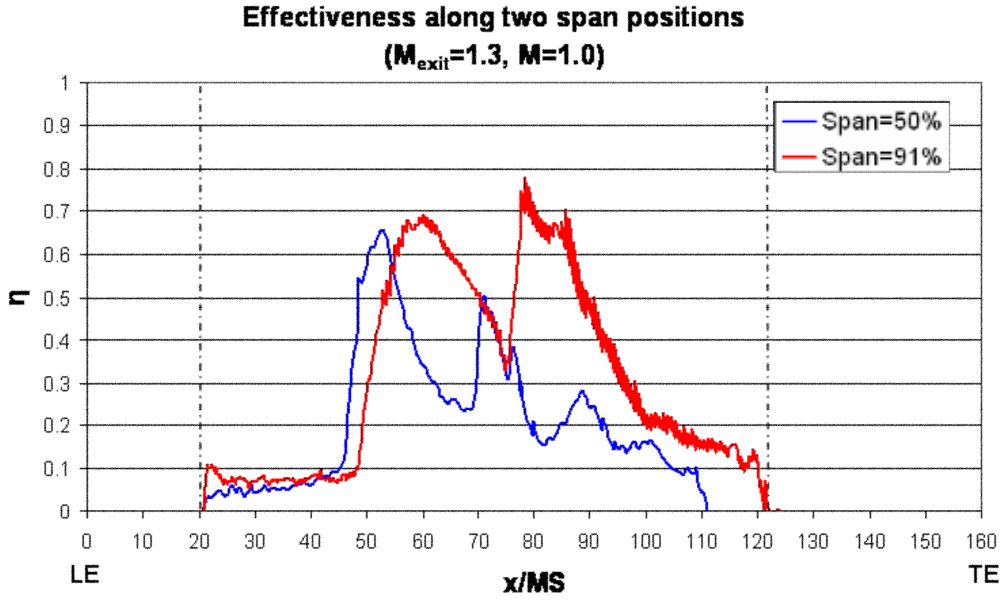

Fig. 51 Effectiveness along two spans position for and exit Mach numbers of 1.3 and blowing ratio = 1.0

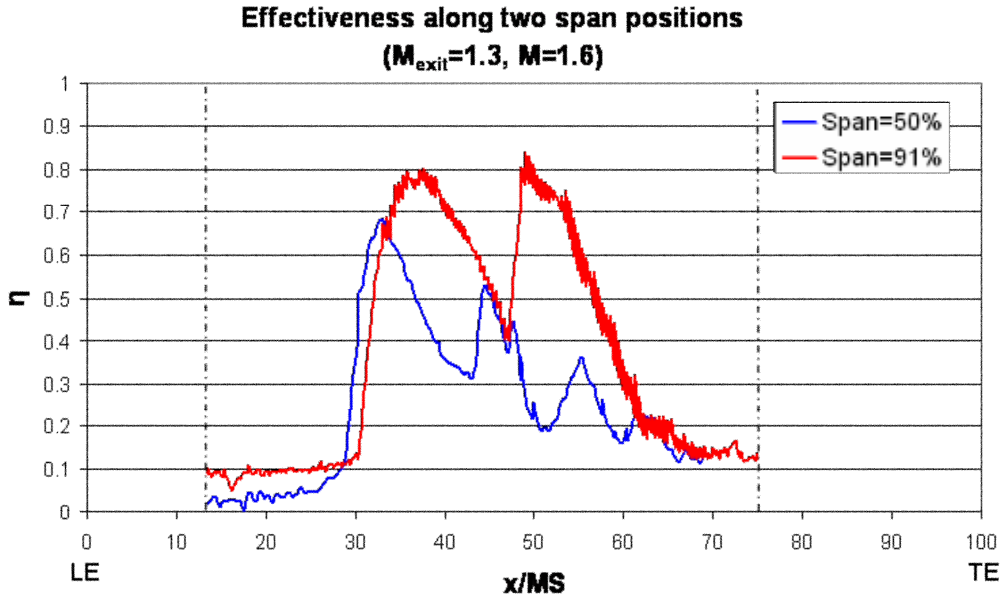

Fig. 52 Effectiveness along two spans position for and exit Mach numbers of 1.3 and blowing ratio = 1.6

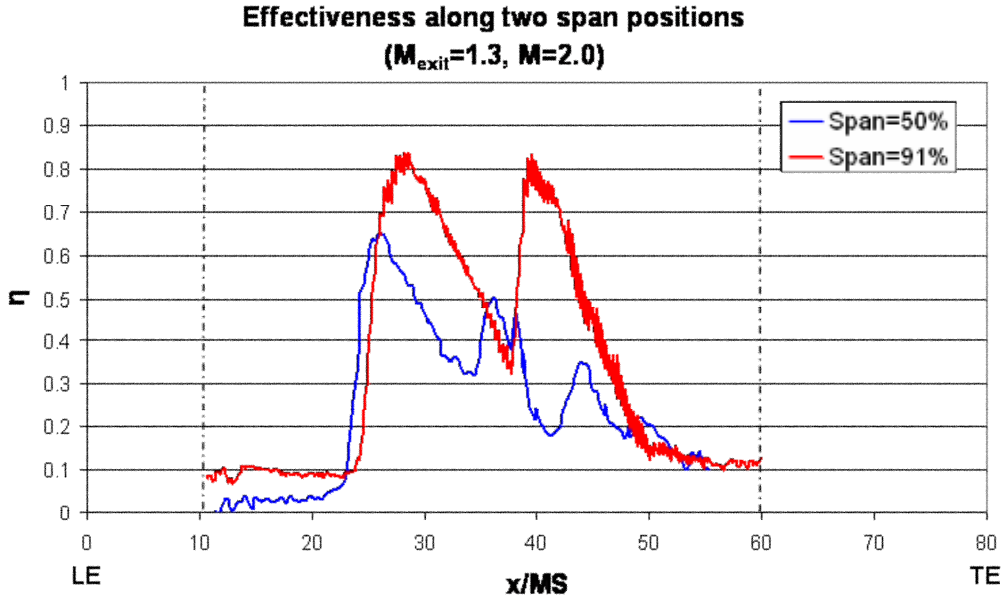

Fig. 53 Effectiveness along two spans position for and exit Mach numbers of 1.3 and blowing ratio = 2.0

Overall Comparison

Figure 54 and Figure 55 show the comparison of the film cooling effectiveness of three different mainstream velocities and four different blowing ratios. At low blowing ratio (M=0.5), exit Mach number = 0.7 has greatest effectiveness follow by the order of exit Mach number = 1.1 and 1.3; as blowing ratio increases, the effectiveness looks similar for supersonic exit conditions.

The spanwise averaged film cooling effectiveness for different exit Mach number and blowing ratios are plotted in Figures 56 to 59. There are two major peaks , which indicates two film cooling holes from row 1 and row 2; at low blowing ratio (before reaching the optimum value), the second peak is higher than the first peak duo to the coolant accumulation downstream. At high blowing ratio (after reaching the optimum value), the second peak becomes lower because the coolant shoot into the mainstream.

The optimum blowing ratio for supersonic exit condition is 1.6; however, the optimum blowing ratio for subsonic condition is 1.0. This is due to the interaction between shock and free stream turbulence. The interaction causes the increasing pressure and assists the coolant to attach on the blade surface at higher blowing ratio; besides, the secondary flow effect decreases as mainstream velocity increases. Thus, the supersonic cases perform better than the subsonic case.

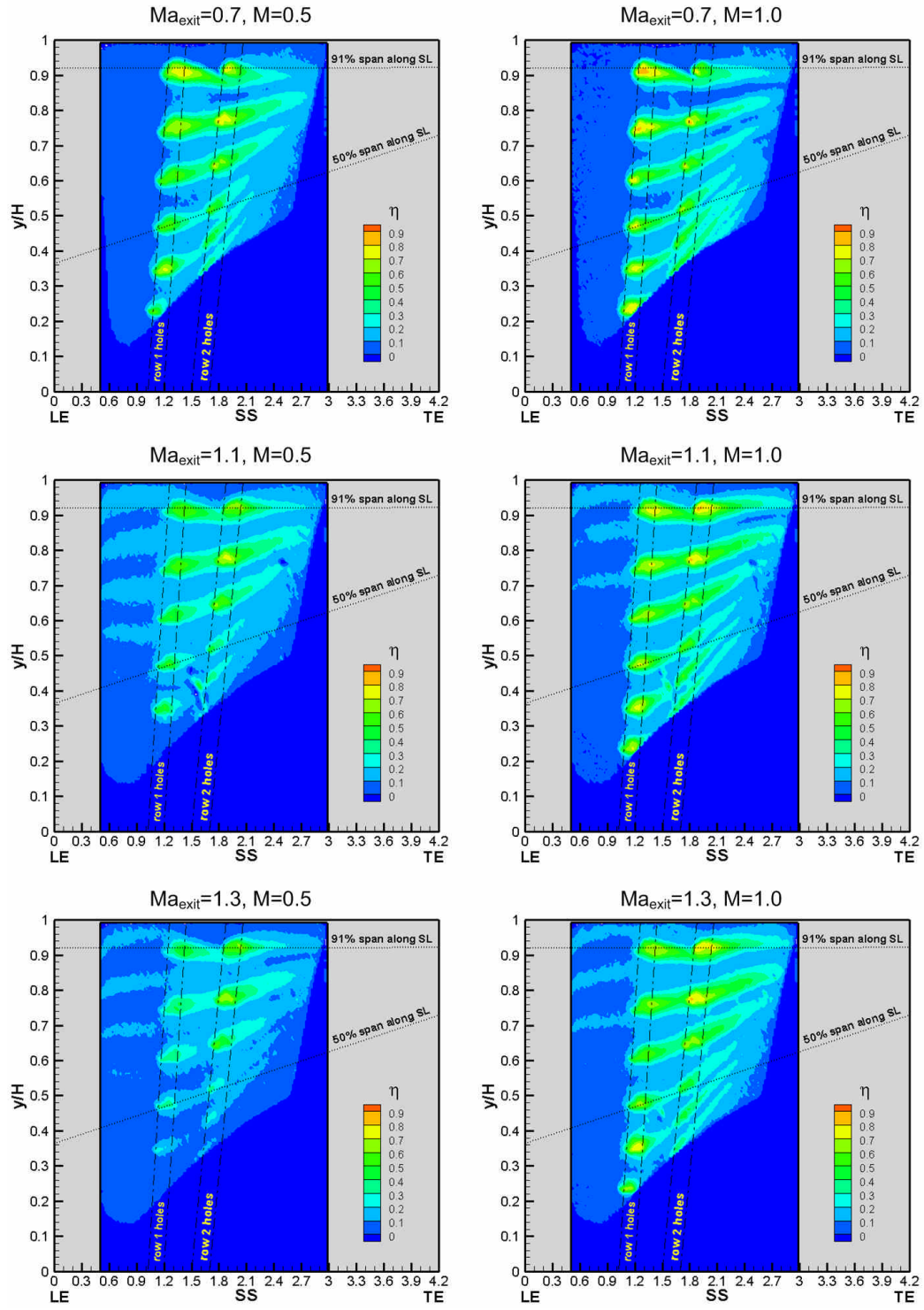

Fig. 54 Effectiveness comparison of exit Mach number = 0.7 to 1.3 and blowing ratio = 0.5 and 1.0

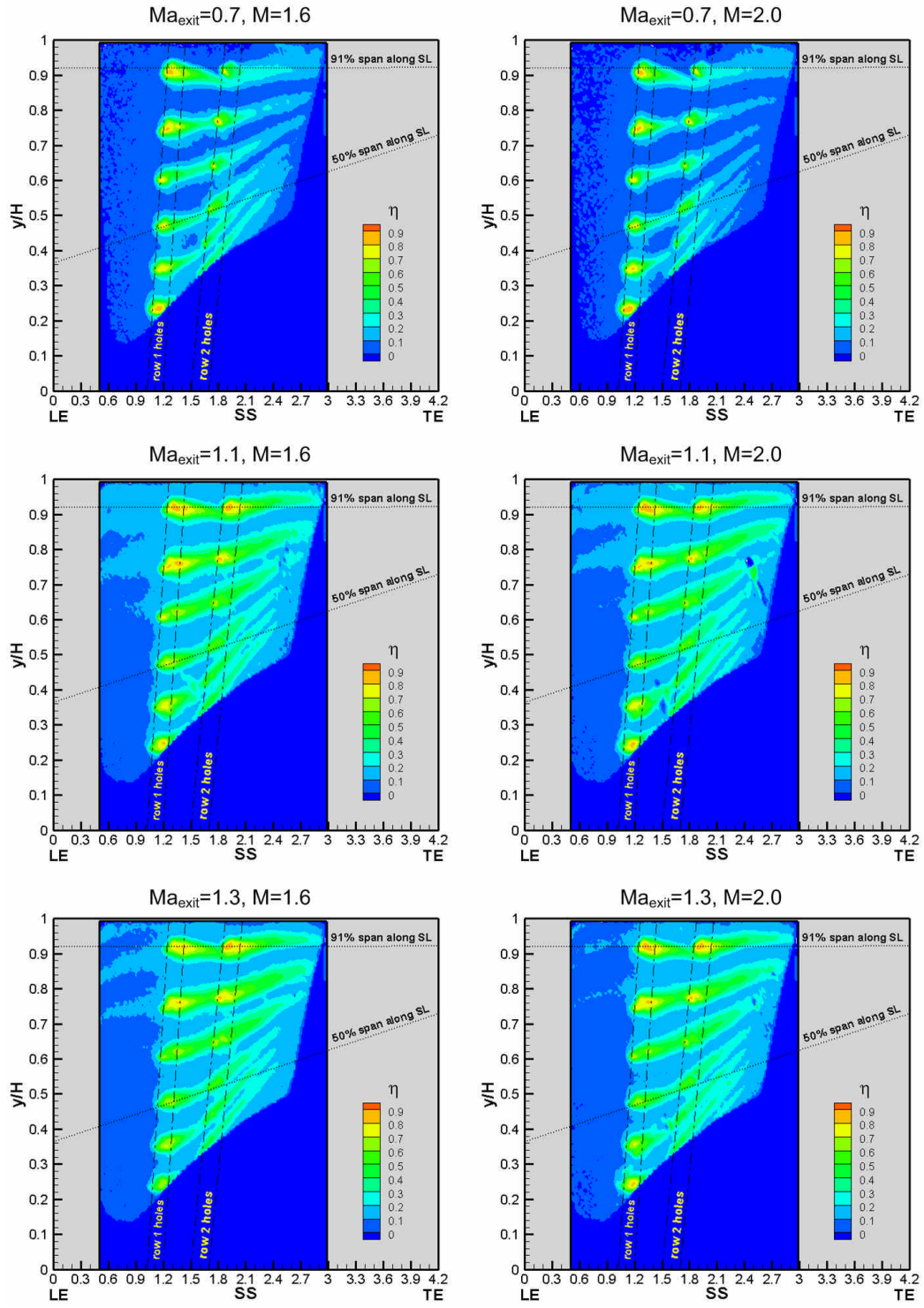

Fig. 55 Effectiveness comparison of exit Mach number = 0.7 to 1.3 and blowing ratio = 1.6 and 2.0

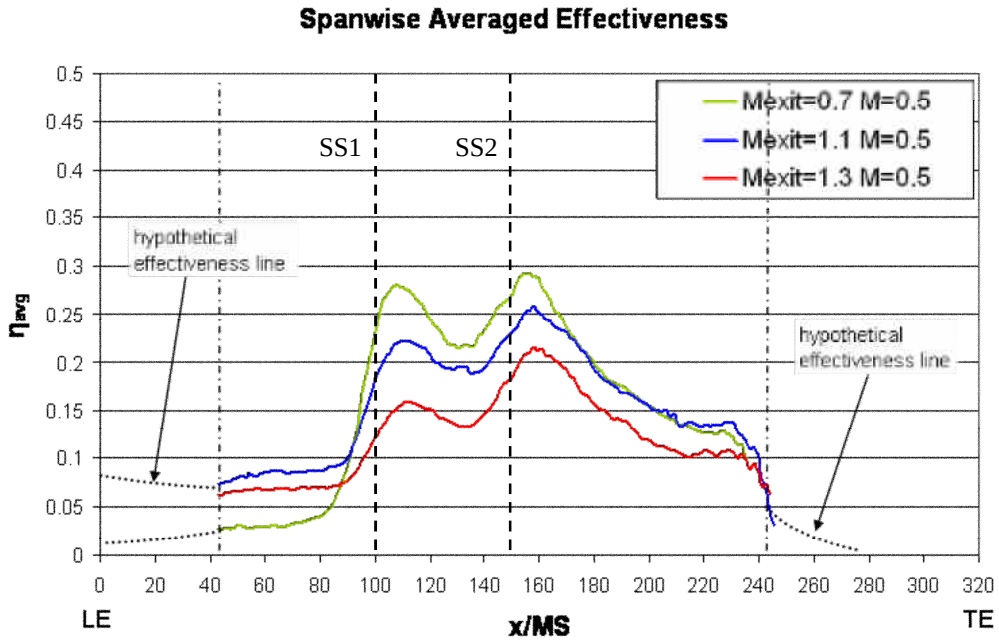

Fig. 56 Spanwise averaged effectiveness comparison of blowing ratio = 0.5

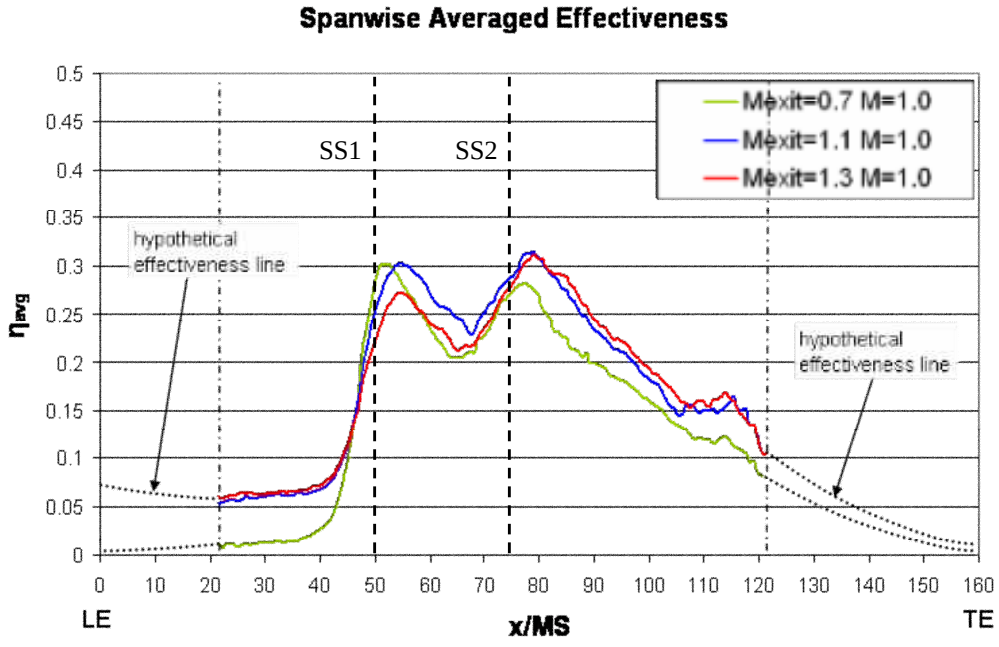

Fig. 57 Spanwise averaged effectiveness comparison of blowing ratio = 1.0

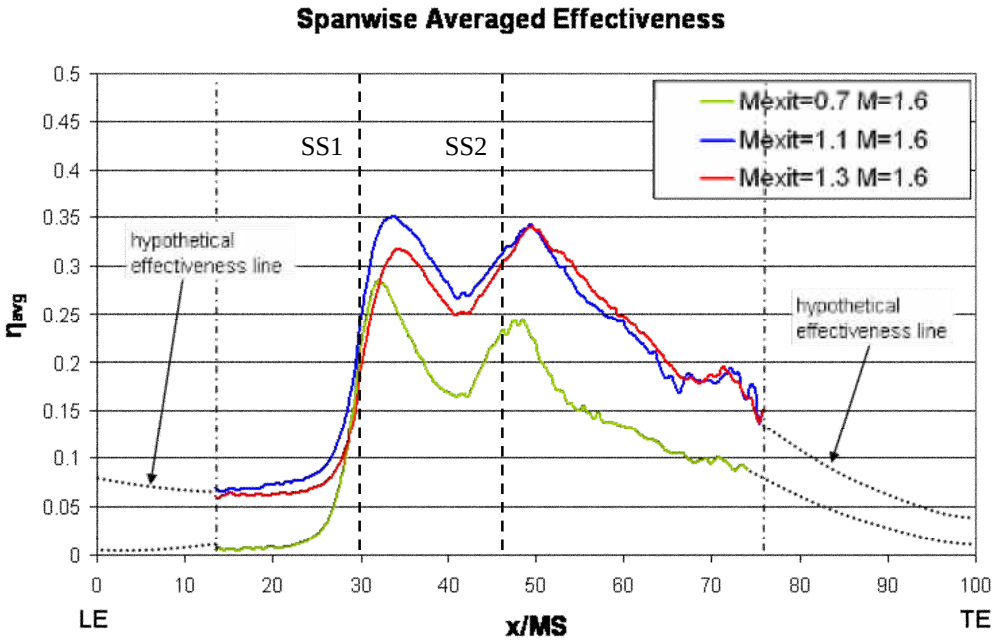

Fig. 58 Spanwise averaged effectiveness comparison of blowing ratio = 1.6

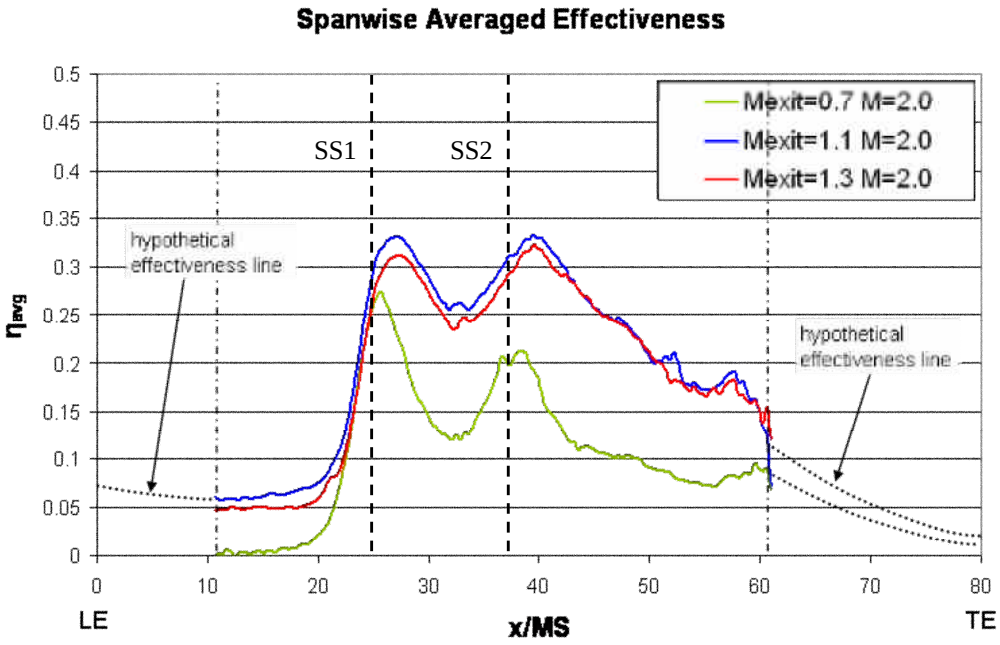

Fig. 59 Spanwise averaged effectiveness comparison of blowing ratio = 2.0

CONCLUSIONS

As exit Mach number becomes 1.1 and 1.3, shockwaves occur at the near-to-trailing edge region and the tail of the coolant trace on the test vane surface. Results show that shocks do not change the trace shape and direction because the coolant dies out before the shocks take place.

On the suction side surface, based on two rows of compound angle shaped holes, the cooling effectiveness increases as blowing ratio increases, till it reaches the critical blowing ratio = 1.0 (for subsonic) and 1.6 (for supersonic). Further increase of blowing ratio causes the coolant liftoff and detach from the vane surface, thus the effectiveness drops. Effects of blowing ratio can also be seen from the 2D line plots by comparing the first and second peak.

As a result of: (1) High pressure caused by shock, not only assists the coolant jet to against the blade surface at higher blowing ratio but also damp the mainstream turbulence . (2) Secondary flow effects decrease as mainstream velocity increases. The optimum film cooling effectiveness happens at M=1.6 (with shock) and at M=1.0 (without shock).

REFERENCES

[1] Han, J.C., Dutta, S., and Ekkad, S., 2000, *Gas Turbine Heat Transfer and Cooling Technology*, Taylor and Francis, New York.

[2] Goldstein, R.J., Eckert, E.G., and Burggraf, R., 1974, "Effects of Hole Geometry and Density on Three Dimensional Film Cooling," Int. J. of Heat and Mass Transfer, **17**, pp. 595–606.

[3] Sen, B., Schmidt, D.L., and Bogard, D.G., 1996, "Film Cooling with Compound Angle Holes: Heat Transfer," ASME J. Turbomachinery, **118**, pp. 800–806.

[4] Schmidt, D.L., Sen, B., and Bogard, D.G., 1996, "Film Cooling with Compound Angle Holes: Adiabatic Effectiveness," ASME J. Turbomachinery, **118**, pp. 807–813.

[5] Thole, K., Gritsch, M., Schulz, A., and Wittig, S., 1998, "Flowfield Measurements for Film Cooling Holes with Expanded Exits," ASME J. Turbomachinery, **120**, pp. 327–336.

[6] Gritsch, M., Schulz, A., and Wittig, S., 1997, "Adiabatic Wall Effectiveness Measurements of Film-Cooling Holes With Expanded Exits," IGTI Conference, Orlando, pp. 97-GT-164.

[7] Yu, Y., Yen, C., Shih, T., Chyu, M., and Gogineni, S., 1999, "Film Cooling Effectiveness and Heat Transfer Coefficients Distributions around Diffusion Shaped Holes," IGTI Turbo Expo, The Hahue, The Netherlands, pp. 97-GT-312.

[8] Gao, Z., Narzary, D., and Han, J., 2007, “Film-Cooling on a Gas Turbine Blade Pressure Side or Suction Side With Compound Angle Shaped Holes,” ASME pp. HT-2007-32098.

[9] Goldstein, R.J., Eckert, E.G., Eriksen, V.L., and Ramsey, J.W., 1970, “Film Cooling Following Injection Through Inclined Circular Tubes,” Israel Journal of Technology, **8**, pp. 145-154.

[10] Cho, H.H., Rhee, D.H., and Kim, B.G., 2001, “Enhancement of Film Cooling Performance Using a Shaped Film Cooling Hole with Compound Angle Injection,” JSME International Journal, Series B, **44**, No. 1, pp. 99-110

[11] Saumweber, C., Schulz, A., and Wittig, S., 2003, “Free-Stream Turbulence Effects on Film Cooling With Shaped Holes,” ASME J. Turbomachinery, **125**, pp. 65-73.

[12] Kadotani, K., and Goldstein, R. J., 1979, ‘‘On the Nature of Jets Entering a Turbulent Flow Part A: Jet-Mainstream Interaction,’’ ASME J. Eng. Power, **101**, pp. 459–465.

[13] Kadotani, K., and Goldstein, R. J., 1979, “On the Nature of Jets Entering a Turbulent Flow Part B: Film Cooling Performance,” ASME J. Eng. Power, **101**, pp. 466–470.

[14] Mehendale, A.B., and Han, J.C., 1992, “Influence of High Mainstream Turbulence of Leading Edge Film Cooling Heat Transfer,” ASME Journal of Turbomachinery, **114**, pp. 707-715.

[15] Burd, S. W., Kaszeta, R. W., and Simon, T. W., 1998, “Measurements in Film Cooling Flows: Hole L/D and Turbulence Intensity Effects,’’ ASME J. Turbomachinery, **120**, pp. 791–797.

[16] Gau, Z.Nazary, D., Mhetras, S., and Han, J., 2007, “Full Coverage Film Cooling for a Turbine Blade with Axial Shaped Holes,” AIAA Paper No. AIAA-2007-3402.

[17] Pedersen, D.R, Eckert, E.R.G., and Goldstein, R.J., 1997, “Film Cooling with Large Density Differences Between the Mainstream ans Secondary Fluid Measured by the Heat-Mas Transfer Analogy,” ASME Journal of Heat Tranfer, **99**, pp. 620-627.

[18] Sinha, A.K., Bogard, D.G., and Crawford, M.E., 1991, “Film Cooling Effectiveness Downstream of a Single Row of Holes with Variable Density Ratio,” ASME Journal of Turbomachinery, **113**, pp 442-449.

[19] Mhetras, S., and Han, J., “Effect of Unsteady Wake on Full Coverage Film-Cooling Effectiveness for a Gas Turbine Blade,” ASME/AIAA Joint Heat Transfer Conference, San Francisco, May 2006.

[20] Mhetras, S., and Han, J., “Effect of Superposition on Spanwise Film-Cooling Effectiveness Distribution on a Gas Turbine Blade,” ASME IMECE 2006-18084.

VITA

Kuo-Chun Liu is from Taipei, Taiwan, and received his Bachelor of Science degree in mechanical engineering from Kansas State University in May, 2007. In September 2007, he began his graduate study in Texas A&M University. While in graduate study at Texas A&M University, he worked in the turbine heat transfer laboratory as a research assistant with Dr. J.C. Han. Liu graduated with his Master of Science degree in mechanical engineering (August, 2009) and is continuing on to pursue his Ph.D. in the same field of study.

Mailing Address:

Kuo-Chun Liu

Department of Mechanical Engineering

c/o Dr. J.C. Han

Texas A&M University

College Station, TX, 77843-3132